Critical Compilation of Surface Structures Determined by Surface Extended X-Ray Absorption Fine Structure (SEXAFS) and Surface Extended Electron Energy Loss Spectroscopy (SEELFS)

Philip R. Watson

Department of Chemistry, Oregon State University, Corvallis, Oregon 97331-4003

Received 4 March 1991; revised manuscript received 1 August 1991

This review critically compiles all surface structures derived by the technique of surface extended x-ray absorption fine-structure spectroscopy (SEXAFS) and surface electron energy loss fine-structure spectroscopy (SEELFS) reported in the refereed literature prior to January 1990. They are compared with the extensive low-energy electron diffraction (LEED) [P. R. Watson, J. Phys. Chem. Ref. Data **16**, 953 (1987)] and ion scattering databases [P. R. Watson, J. Phys. Chem. Ref. Data **19**, 85 (1990)] previously reported. The important experimental and theoretical aspects of such investigations have been extracted into easily understood tabular form supplemented by many figures and ancillary tables and complete references. It is hoped that this compilation will provide a valuable resource both for the surface science specialist and for those nonspecialists in other areas who need surface crystallographic data.

Key words: critically reviewed data; surface extended x-ray absorption fine-structure spectroscopy; surface electron energy loss fine-structure spectroscopy; surface crystallography; surface structure

Contents

List of Tables

List of Figures

1. Introduction

1.1. Background

A knowledge of the properties of surfaces at the atomic level is becoming increasingly vital for a better understanding of the operation of microelectronics circuits, the action of catalysts, and the microscopic details of metallurgy, tribology, and corrosion. Hence, surface science investigations are destined to play an increasingly important role in many areas of technology. Of all the types of information concerning a surface that we may wish to obtain, a detailed surface crystallography is perhaps the single most important item. A reliable surface structure provides the starting point from which the behavior of the surfaces of materials can be explored.

A number of techniques that are sensitive to the atomic geometry of surfaces have been developed, using electron, photon, and ion probes. The most widely used of these have been low-energy electron diffraction (LEED) and ion-scattering methods; they have been the subjects of two previous critical compilations[1,2] in this series. These techniques have been extensively deveoped over the last two decades, and have provided numerous surface crystallographies of clean and adsorbate-covered systems. The technique of surface extended x-ray absorption fine-structure spectroscopy (SEXAFS) is rapidly becoming an increasingly important source of surface structural data. It has developed more lately than LEED or ion-scattering because of the need for a high-brightness synchrotron radiation source for this type of spectroscopy. A variant of this technique, surface electron energy loss fine-structure spectroscopy (SEELFS), which employs electrons rather than x rays as the excitation source, obviates the necessity for a synchrotron source, yet provides similar information. The theoretical underpinnings of this technique have only recently been worked out, and not many systems have been investigated up to this point.

A number of reviews of SEXAFS[3–11] and SEELFS[4,12,13] have appeared, of varying degrees of detail. Two of the most complete SEXAFS reviews are those of Citrin[6] and Stohr,[3] written in 1986 and 1988, respectively, while De Crescenzi has recently completed a major article on SEELFS.[12] The compilation presented here is distinguished by providing a detailed, critical summary of all the refereed SEXAFS/SEELFS studies that have reported useful surface crystallographic data through January 1990. In particular it provides a survey of surface structural results that has been critically examined as to the accuracy and internal consistency of the quoted results. These are presented in a condensed, but easily understood, database format. In addition, where possible the results are discussed and compared with existing LEED or ion-scattering structures. It is hoped that this survey will be a valuable resource not only for specialists in surface science, but also for workers in other disciplines that need surface structural data to understand and extend their work, yet lack the time or resources to evaluate the complex and interrelating factors that contribute to the derivation of a structure quoted in the literature.

1.2. SEXAFS/SEELFS in Comparison with Other Techniques

It is instructive to briefly compare the characteristics of the principal surface crystallographic methods. Experimentally LEED and SEELFS are within the reach of any laboratory, requiring only modest equipment. Ion-scattering meth-

ods need more complex apparatus, increasingly so with the energy of the ion used. SEXAFS can only be sensibly performed at an electron storage ring where the necessary photon fluxes in the x-ray region of the spectrum are available. Although photon fluxes are continuously being improved, most SEXAFS experiments have required much longer collection times (many hours) than LEED, SEELFS, or ion scattering (minutes to hours).

The fine-structure techniques have traditionally employed a Fourier transform data analysis approach that yields a unique crystallographic solution with relatively little computational effort. We can contrast this situation with the often massive multiple scattering calculations needed in LEED investigations that proceed via a trial-and-error comparison with postulated structures. The situation in this area is, however, less clearcut when a mutlishell appoach (*vide infra*) to SEXAFS data analysis is needed, and a unique solution is no longer simply available.

The size of the datasets used in structural determinations with these different methods vary dramatically. LEED practitioners have sought to increase the accuracy of their structures by recording large numbers of diffracted beams, perhaps 20 +, at several angles of incidence. A similar trend to record larger and larger datasets is apparent in the ion-scattering literature.[2] In general SEXAFS structures have been determined from just one set of data via the Fourier transform, or possibly from polarization-dependent data taken at a small number (typically $\leqslant 3$) angles.

The great advantage of SEXAFS and SEELFS as surface structural tools, in contrast to LEED, is that they do not require long-range order and hence can be used to investigate a wider variety of systems. The other side of the coin is that the short-range nature of the technique means that it usually cannot provide information much beyond the first coordination shell of a surface atom. It is also difficult for these techniques to distinguish the signal originating from surface atoms from that coming from bulk atoms of the same material. The fine-structure techniques are best suited to investigation of adsorbate systems where the atomic charges of the adsorbate and substrate are quite different.

Hence, in many ways SEXAFS is a complementary tool to LEED. While LEED requires long-range order, this necessity allows the determination of the interior structure of the surfaces of metals and semiconductors, a region largely inaccessible to SEXAFS. On the other hand, many adsorbates form poorly ordered surface phases that are better suited to a SEXAFS analysis, with the added benefit of not requiring the large computational effort typical of a LEED investigation.

The investigation of molecular adsorbates is an obvious area of expansion for all the surface structural techniques. SEXAFS and SEELFS would seem to be well suited for such investigations, but there exist a number of difficulties which have slowed this application. The principal problem is that many molecular adsorbates are fragile, being very susceptible to electron, ion, or photon beam damage. Also, the analysis of the fine-structure data can run into problems when there are several closely spaced shells of atoms surrounding an adsorber. It is possible that improvements in photon sources and detectors may be necessary before such investigations are possible.

1.3. Organization and Scope

The body of the review is organized as follows. First we very briefly review some of the basic aspects of SEXAFS and SEELFS experiments pertinent to understanding the structure of the compilation. This is particularly intended for those readers not familiar with this topic; more complete accounts can be found in the reviews referred to therein. Next we examine in some detail the various components that go into a surface structural determination by these methods, and we attempt to establish criteria that would give us a reasonable degree of confidence in the derived result.

The compilation of surface structures is presented in the form of a large table (Table 1), showing the most important experimental and theoretical parameter values, and a brief description of the results of the study. Further discussion of some of the reported structures follows in Sec. 5. The discussion section contains a number of accompanying notes, figures, and ancillary tables. These serve to amplify and clarify the brief descriptions given in the main table. Where possible we compare the SEXAFS/SEELFS results with those from well-established LEED and ion-scattering studies. However, in the interests of brevity, we do not fully discuss these latter data, only the best-accepted results. Readers who require more information on these surface crystallographic structures are urged to refer to the previous compilations,[1,2] and references therein.

The temporal scope of this review covers surface structures reported in the refereed literature since the inception of modern investigations, roughly 1977, until January 1990. The scope of the compilation has also been deliberately limited in other ways. The first is that in order to ensure the reliability of the compilation, only papers appearing in regular peer-reviewed journals were considered; articles published in unrefereed conference proceedings or society bulletins are not included.

Second, the review is restricted as much as is feasible to "true surface structures"—that is to studies that result in the finding of the atomic coordinates of atoms in the first few atomic layers of a solid. This approach provides a natural continuity with the previous compilations. Hence, investigations dealing with the structure of buried interfaces, or defects in thin films, are excluded. In this regard, for the purposes of this review we shall not use the term "structure" to mean a completely determined geometry, in the sense that an x-ray crystallographer might understand the term. Surface crystallography has not advanced to that highly automated level of development. Rather we interpret "structure" in the broadest sense to mean a report of a surface geometry that may be fragmentary and incomplete, but still advances our understanding of the system.

Third, where the same group of investigators has reported several times on the same structural problem (perhaps in increasing levels of detail), the results have been consolidated into one table entry. However, in such cases all the references are supplied.

Another x-ray technique that exploits a different area of the absorption specturm—near-edge spectroscopy (NEXADS), sometimes referred to as x-ray absorption near-edge spectroscopy) (XANES)—is not included in this compilation. It is a developing technique[8,9,14] that is proving useful for investigating the electronic nature of an adsorbing atom, and can, in some cases, identify adsorption sites and molecular adsorbate orientations. The method of data analysis and spirit of NEXAFS is quite different from that of SEXAFS or SEELFS and has not yet often yielded specific surface geometrical information. Hence at this time it is not appropriate to include NEXAFS studies in this compilation.

2. THE SEXAFS and SEELFS Techniques

2.1. Introduction

There are many techniques available that are sensitive to one or another structural aspect of a surface. They can be generally divided into two groups—those that are long range, and those that are short range in nature. Low-energy electron diffraction is an example of the long-range type of surface structural technique, where a crystalline material having a high degree of surface order over many lattice spacings is necessary to produce a useful diffraction pattern. This requirement makes high demands upon experimentalists, but does have the benefit that distortions that propagate several layers deep into the surface can be investigated.

Ion scattering, SEXAFS, and SEELFS exemplify short-range techniques. As a corollary of their short-range nature, these methods are less useful for investigations of near-surface reconstructions. The latter two techniques owe their surface structure sensitivity to the near-neighbor scattering of secondary electrons emitted by an atom that was originally excited by an electron (SEELFS) or x-ray photon (SEXAFS). In this sense the origin, and indeed the mechanics, of obtaining structural results from SEXAFS or SEELFS data are quite similar. In general it is difficult to detect scattering from shells of atoms more than a few Å distant from the absorbing atom. Hence, SEXAFS and SEELFS have the advantage of not requiring long-range ordered surfaces, but do require a uniform type of bonding at the surface, or they will only report an average structure. However, as we shall see, the majority of SEXAFS and SEELFS studies have to date been carried out on single crystal substrates.

2.2. SEXAFS Experiments

SEXAFS is of course the surface variant of bulk EXAFS, which has a long history of providing crystallographic data in amorphous materials.[15] Appropriately, SEXAFS shares some of the technical aspects of EXAFS although special experimental techniques are necessary to obtain surface, as opposed to bulk, information. The usual mode of analysis of SEXAFS spectra is borrowed almost unmodified from that of traditional EXAFS.

Bulk EXAFS is at heart an absorption spectroscopy; the experiment measures the reduction of intensity of an x-ray beam, via the absorption coefficient μ, after passing through a thin sample. The absorption coefficient is strongly dependent on photon energy in the region about the core ionization energy of an atomic species in the sample. The coefficient generally rises sharply at the absorption edge, while at some distance above the edge oscillations, or fine structure, occur which give the technique its name. These oscillations originate in the interference between photoelectrons directly leaving the absorbing atom with others that have backscattered from surrounding atoms.

This kind of bulk transmission experiment cannot usually yield sufficient surface sensitivity to detect effects due to the outermost atomic layers, except possibly in supported catalysts, where essentially all the atoms of interest are at the surface. To make the method surface sensitive we can monitor the photoionization event, not directly through the absorption of a photon, but through other secondary processes due to filling of the primary core hole created by the photon. Stohr[3] has considered the pros and cons of SEXAFS detection methods in detail.

A particularly useful monitor of the photoionization process are Auger electrons generated when the core hole is filled. If these originate from within a few Å of the surface, they will emerge unscattered with an energy characteristic of the absorber atom. If the Auger electrons are released from deeper in the solid, they will suffer inelastic losses and contribute to the background secondary yield. The Auger signal is thus very surface sensitive and monitoring the change in Auger electron signal corresponding to a particular element of interest as the photon energy is swept through the absorption edge can yield a SEXAFS spectrum—we will denote this as the Auger yield (AY) method. Measuring the Auger signal necessitates a dispersive spectrometer with rather small acceptance angle, and hence, a low signal-to-noise ratio. Many experiments have been performed using the partial or total secondary electron yield (PY or TY), which yields the same spectra with more signal, but a reduced signal-to-background ratio compared to AY.

A second way of monitoring fine-structure modulations is to measure the fluorescence yield (FY) arising from filling of the core hole. This method is particularly useful for low-Z elements (with $Z < 30$) which have low Auger yields. Here surface sensitivity must be achieved by the use of glancing incidence angles. Only a few instances of this type of measurement have been reported for surface systems. Another detection scheme that has been tried is photon stimulated ion desorption (PSID) resulting from hole decay.[16]

Unfortunately, the fine-structure oscillations observed in these experiments are typically only about 1% of the total signal. If we couple this with a wish to be able to detect the element even if it is only present in the surface at levels of a few percent, then the need for an extremely bright radiation source, such as a synchrotron, is apparent.

2.3. SEELFS Experiment

The practical difficulties of having to perform SEXAFS experiments at a central synchrotron facility have led to attempts to exploit electron scattering originating from electron rather than photon ionization. Not only can electron sources be easily constructed, but they open the possibility of

spatially resolved experiments due to the ease of focusing and scanning electron beams in comparison with x-rays. However, the basic physics of the interactions is rather different. Whereas a photon will give up all its energy in the absorption process, an incident electron may only give up part of its energy to the bound electron. The result is that a large number of two-electron final states are possible that still conserve the total energy. Hence, we can expect fine-structure interference effects in the total electron ionization cross section involving both electrons.

A solution to this problem is to measure a differential cross section by setting the incident electron energy sufficiently far above the threshold for ionizations that the EXAFS modulations for the incident electron, even after ionization, are damped to the point where the signal is essentially due solely to the final-state scattering of the ionized electron. Such an arrangement has the added advantage that the interaction of the incident electron is dipole-like with dipole selection rules.

The SEELFS experiment thus consists of using a high-energy incident electron beam and energy analyzing the scattered electrons to detect oscillations in the energy-loss spectrum above an ionization edge. The fine structure is isolated by synchronous lock-in amplifier detection at the frequency of the modulation applied to the sample and, for instance, to the cylindrical mirror analyzer (CMA) bandpass energy. This technique also helps to eliminate Auger signals overlapping the true energy loss spectrum. Ideally the experiments should take place in a reflection mode at incident energies of 100's of keV to fulfill the conditions outlined above. However, the more usual surface science instrumentation, such as CMA and concentric hemispherical (CHA) analyzers, operate more typically at a few keV. As a result, most SEELFS experiments have used primary beams of lower than optimal energy for a true separation of the one-electron final states and a dipole excitation mechanism; nevertheless, the results to date are encouraging.[12]

Perhaps the most limiting aspect of SEELFS experiments is the relatively large beam doses that result from currents that are often several μA in magnitude. For the investigation of the surface layers of bulk materials or atomic adsorbates such beam currents usually cause little in the way of beam damage difficulties. However, such doses are more than sufficient to cause extensive beam-induced desorption or reactions of molecular adsorbates, thus restricting the range of the applicability of the technique.

2.4. Data Analysis

We here present a brief unified account of the essentials of the data analysis procedure common to both the x-ray and electron-excited techniques. Much fuller accounts are widely available.[3–15] The fine-structure signal is defined as the relative difference of the ionization cross section for the atom in the surface, μ, to that of a free atom, μ_0:

$$\chi(k) = (\mu - \mu_0)/\mu_0.$$

In practice μ is usually taken as a smooth fit (often spline-polynomial) through the oscillatory structure above the edge.

We can also express this measured quantity by the theoretical expression.[17,24,25]

$$\chi(k) = (-1)^l \sum_i^n A_i(k)(2k \sin R_i + \phi_i^l).$$

Here l is the dominant partial wave component of the final state wave function determined by dipole selection rules, i.e., $l = 0$ for s states (K,L_1 edges) and $l = 1$ for p states (L_2 or L_3 edges). The expression is summed over all n shells of atoms i at distance R_i from the absorber. The remaining terms are the total amplitude A_i and a k-dependent phase shift $\phi(k)$ that the scattered electron experiences due to the absorbing and scattering atoms.

In the case where the neighbor shell contains N_i identical atoms, the amplitude function can be written in the harmonic potential approximation as:

$$A_i(k) = (N_i^*/kR_i^2)F_i(k)\exp(-2\sigma_i^2k^2) \times \exp[-2R_i/\lambda(k)].$$

Here $F_i(k)$ is the backscattering amplitude of the neighboring atoms, while the first exponential terms account for thermal disorder via a Debye–Waller expression, and the final term approximates for inelastic losses through the mean-free path of the photoelectron λ. As Gamble and King have pointed out,[18] in some systems anharmonic effects may lead to systematic errors through the use of these equations. They have shown that an anharmonic function[19] used with low-temperature data can be successful.

The structural quantities of interest in these experiments are therefore the distances and number of atoms coordinated to the absorber in the ith shell. In order to do this, we need as input details of the amplitude and phase functions and Debye–Waller factors, although these could be treated as unknowns to be determined. There have been two methods used to extract structural parameters from raw χ data. The most common is to take the Fourier transform that will contain peaks at distance R_i^* which differ by a phase shift from the true shell separation. The contributions from each shell can be separated out using a windowing function and the data backtransformed to k space to isolate the amplitude and phase functions for each shell. We will refer to this as the single-shell (SS) procedure. The experimental phase shift is either assumed to be the same as that in a closely similar model compound—using the concept of "phase shift transferrability"[20]—or taken from theoretical tabulations.[21–24] It is subtracted from the R_i^* to yield the interatomic distance. The coordination number requires a comparison of the amplitude function with a model system. This amplitude transferability is generally less successful than that for the phase shift and limits the accuracy in favorable cases to about 10%.[25] Alternatively, because N_i^* depends on the angle between the electric field vector of the photon beam and the interatomic vector, a ratio of amplitudes taken at two angles of incidence can sometimes be successfully used to find the symmetry of an adsorption site.

The second analysis method is to curve-fit directly a multishell (MS) analysis to the original background-sub-

tracted data. Although MS methods have been in use in bulk EXAFS experiments for many years, they have only recently been employed in the surface analog.[18] Here calculated phase shifts are used, though they are typically iterated to give the best fit to model compounds, along with other reasonable estimates of the mean-free path, Debye–Waller factors, etc.

3. Evaluation Criteria

Before an investigator can attempt to determine a surface structure by any surface structural technique, there are a number of standard procedures that must be followed. Extended fine-structure investigations are no exception to this rule. Thus, the surface must be prepared to expose the surface, and plane in the case of single crystal substrates, of interest with an acceptable levels of impurities. Any desired adsorbate must be introduced onto the surface. Once the surface is prepared in the desired state, the data must be collected, and the structure derived via an appropriate theory. Each of these stages of experimentation and analysis has associated with it certain problems that may affect the reliability of the result and can involve judgments that may be open to more than one interpretation.

Hence a proper critical evaluation of a surface crystallographic study involves a consideration of many different factors, which may have complex interrelationships, that can affect our confidence in the reported result. Given the many diverse components that go into a complete study, and the many factors that can influence the reliability of a given result, it is difficult to come up with some simple numerical index that would signify a "good" or "bad" structure. The most realistic solution to providing a confidence level for a given result is to draw up a list of criteria that would define a very reliable study. In some instances a criterion might indeed be numerical—a contamination level as percent of a monolayer, or the number of datasets used in a comparison of theory and experiment. Sometimes it may only be possible to reveal unquantifiable misgivings about some aspect of the procedures—for instance doubts as to a careful avoidance of disturbing effects such as radiation damage.

The approach used here for critically evaluating SEXAFS and SEELFS data will focus on the most critical areas of the technique—sample preparation, data collection, and analysis. Therefore, we will now examine each step of a typical experiment and discuss the factors that affect the results. The criteria that are developed here form the basis for the columns reported in the main database table and should be read before using the table for a proper understanding of their meaning and function.

3.1. Surface Preparation

The preparation of the surface under study is such a fundamental part of any surface crystallography experiment that it is incumbent upon us to make a critical examination of the described procedures. The first goal of any surface science experiment is to prepare the surface under consideration in the required form. Single crystal samples, which form almost all the reported cases, are usually cut from a rod or boule, oriented and polished using standard metallographic methods, and mounted on a manipulator. With care the orientation of the polished crystal should be within 1°, or less, of the desired plane. Few workers, however, explicitly state that they check that the x-ray face, as found from a back-reflection Laué photograph, is parallel to the polished optical face. This can be easily done using a small He–Ne alignment laser. As the metallographic techniques for preparing a polished crystal slice of a particular orientation are standard procedures, we assume here that the sample is oriented to within 1°, unless the authors state otherwise.

The contamination and damage introduced during the cutting and polishing processes is usually removed by cleaning the surface to some acceptable level of contamination, using thermal, chemical, or ion-bombardment techniques. Chemisorbed structures can then be obtained by adsorption. Analytical techniques[26] such as Auger electron spectroscopy (AES) or x-ray photoelectron spectroscopy (XPS) can reveal adatom concentrations at the level of a few percent of a monolayer coverage, and form useful adjunct techniques.

The question of what constitutes a clean surface is of course a vexed one, and can depend very much on the system, and on the requirements and sensitivity of the experiment. Thus it is much more difficult to produce a truly clean iron or titanium surface, than a copper or gold surface. Furthermore, surface reconstruction might be turned on or inhibited by small amounts of contamination. Accordingly, it is suggested here that we adopt the (generous) figure of 5% of a monolayer to represent an upper bound to an acceptable contamination level in ordinary circumstances.

Of necessity, LEED surface crystallography studies have been carried out on well-defined highly ordered surfaces. Due to the local nature of the SEXAFS and SEELFS experiments, this restriction disappears. However, many such studies have been performed on systems that are known to form ordered structures; in some cases this is merely assumed to be the case. It is most reassuring to know that the experimental data are in fact from the same structure that have been studied by other methods. For this to be the case, some means has to be provided to assess the surface order. The natural tool to have available is LEED optics in order to provide a qualitative check on the symmetry and order of the surface under examination. In the absence of any well-defined quantitative measure of surface crystallinity, workers generally rely on a visual judgment of a low background coupled with small, sharp diffraction spots to indicate a well-crystallized surface.

Thus, in the area of surface preparation we can formulate the following criteria for effective preparation:

- The contamination level should be below 5% of a monolayer as measured by ancillary analytical methods. Spectra or quantitative data should be reported.
- Ordered structures should be checked with LEED and the degree of crystallinity estimated, preferably with photographs.

To be fully assured of adequate surface preparation we should be able to give an affirmative answer to these questions. In fairness, however, it would be sufficient for an au-

thor to refer to a previous paper in which these details have been covered.

3.2. Data Collection

3.2.a. Amount of Experimental Data

The quality of a SEXAFS or SEELFS structure is determined to a large extent by the amount of data available. If the range of k space covered is too small then artifacts may appear in the transformed data caused by truncation errors and long period oscillations may be obscured. A common figure of merit seen in the literature is that at least 300 eV of data starting from about 60 eV above the edge should be accessible, although for low-Z absorbers, i.e., for $Z < 10$, perhaps 400 eV would be a preferable number.

Unfortunately, several complications can make attainment of these goals difficult. The most obvious problem is that of interference from absorption edges other than that under investigation, e.g., L_2 and L_3 edges. A second difficulty can arise from a substrate or adsorbate photoemission peak being swept through the detector window with increasing photon energy. A final possible complication is that of standing-wave interference peaks, or Bragg "glitches," which can cause sudden changes in the adatom photoadsorption. Citrin[6] and Stohr[3] have considered in some detail the best methods of data collection to avoid such problems.

In cases where experiments are exploiting the angular anisotropy of the fine-structure signals to determine adsorption sites or orientations it is clear that data must be acquired for at least two angles of incidence. The number of angles actually used should of course be reported; clearly three or more angles provides for an increased reliability of the results.

3.2.b. Signal Considerations

Let us consider the situation for SEXAFS first. The quality of fine-structure data is vitally influenced by two types of signal characteristics. The first of these is the signal-to-background, or edge jump ratio (J_r), defined as:[3]

$$J_r = (I - I_b)/I_b = (I_s/I_b),$$

where I is the incident-flux-normalized total count rate at the absorbing atom edge, I_b the background count at some small energy above the edge, and I_s the surface signal. For a given system the fine-structure amplitude is a fixed fraction of the edge jump, hence it is desirable to make J_r as large as possible to emphasize the fine-structure modulations most effectively. The second quantity of interest is the signal-to-noise ratio (SN):

$$\mathrm{SN} = I_s/\sqrt{I},$$

which we clearly wish to be as large as possible. The size of the edge jump and the SN ratio are both determined to a large extent by the measurement method employed, as has been discussed by Stohr.[3] The correct choice of detection scheme is a major element in the strategy of planning an SEXAFS experiment, especially as the characteristics of the system under study may also impose limitation such as interfering absorption edges.

The other factor underlaying these considerations is the effective photon flux in the sample area. Low fluxes will allow time for sample degradation and drifts in the beam or monochromator optics to occur during the accumulation of sufficient counting statistics. Citrin[6] proposed the figure of 5×10^{10} photons/s striking the sample area as a minimum flux to allow 0.3% statistics (10^5 counts/point) to be collected in less than 12 h of accumulated scanning. This length of data collection is rather long by comparison with other surface structural techniques; for instance LEED measurements are routinely made in matters of minutes. It would seem that to truly avoid the complications of long collection times, fluxes of 5×10^{11} photons/s would be more preferable. Until recently such a high brightness was difficult to obtain even from a synchrotron light source, but recent advances in storage ring technology promise much greater brightnesses in future.

For SEELFS the major difficulty is in obtaining a good signal-to-noise figure. As the electron flux can be increased almost arbitrarily within the constraints of sample damage by increasing the beam area, the quality of the spectra depends to a large extent upon the modulation voltage used and the exact detection scheme. Typical experimental conditions that produce good spectra are in the range of 5–10 V modulation voltages, and 1–10 μA beam current for data collection times of less than 1 h.

We can summarize the above discussion into the following data collection criteria:

- Incident beam fluxes should be of the order of 10^{11} photons/s in the sample area (SEXAFS) or a few μA of electron current (SEELFS).
- Fine structure should cover a range of at least 300 eV (400 eV for $Z < 10$).
- Polarization data should be taken for at least three angles of incidence.

3.3. Data Analysis

The large majority of investigations to date have used the Fourier transform approach to data analysis employing phase shifts either from calculations or transferred from model compounds. Clearly the closer a model compound is to the actual system under scrutiny, the more accurate will be the structural determination. Significant inaccuracies can occur if the atomic charge differs by more than two units between the surface atoms and a convenient model reference.[26] Similarly, care must be taken if linearly parametrized phase shifts are employed; phase shifts are not exactly linear functions, and the typical operations performed during analysis tend to magnify errors. As stated earlier the use of absolute amplitudes is generally not as reliable as using polarization-dependent data.

The area where fine-structure techniques run into the most difficulty is when two or more bond lengths from different shells are similar, for instance less than 1 Å. Strangely, if the distances are closely alike, say of the order of 0.2 Å, then a single shell analysis with averaging can still be effective. In general, in cases where multiple similar bond lengths occur, which include many important surfaces such as semi-

conductors, open metal planes, and molecular adsorbates in low-symmetry adsorption sites, multishell fitting is the best approach. Here too the accuracy of the result depends critically on the data quality. Also, care must be taken to avoid false minima, and that a sufficient volume of parameter space has been searched.

We might note that there appears to have been no discussion in the literature of the best method of assessing the degree of fit between calculated multishell analyses and experimental data. A least-squares analysis seems to be the only method in use. This is in marked contrast to the ion-scattering, and particularly to the LEED communities where a number of reliability factors have been proposed for this purpose. This is curious in that the type of data to be analyzed for SEXAFS are smoothly varying curves with some similarity to LEED intensity–voltage curves, although LEED datasets are usually much larger.

In order for readers to assess the reliability of a particular study, authors then need to clarify the following issues:

- The source and treatment of any calculated phase shifts.
- If model compounds have nuclei with nuclear charges within two units of those under study.
- That the values of any fixed nonstructural parameters such as inelastic mean-free paths are given in a multishell analysis.

3.4. Overall Assessment of Reliability

Having enunciated several criteria for estimating the degree of confidence we find in a particular structure determination, it remains for us to try to find a way to wrap all these different factors into one overall assessment of the confidence level of the structure. This is very difficult to do because of the varied nature of the different criteria and the lack of a numerical basis for distinguishing conflicting results. Based on the literature consensus it is likely that fine-structure studies that have a sufficient range of data and fulfill the other requirements set out above are repeatable, that is, have a precision, to 0.01 Å or better. The question of accuracy, that is, how closely does the result reflect reality, is perhaps best approached by searching for systems where the SEXAFS and SEELFS results can be compared with those from other techniques. We will discuss this after the presentation of the results of the compilation.

This critical compilation presents the reader with a complete picture of a particular study in a very condensed form in Table 1. It is arranged so as to allow the reader to easily and quickly find a structure. The reader will quickly be able to form a judgment as the extent that a particular study has fulfilled the criteria suggested above. Table 1 is followed in Sec. 5 by an expanded discussion with numerous figures and ancillary tables.

4. Surface Structure Compilation

4.1. Organization and Nomenclature

Table 1 presents the surface structure compilations. It contains values of the pertinent experimental and theoretical parameters discussed earlier in a concise, but easily understood form. Also Table 1 shows structural and nonstructural parameters derived from the experimental data. In addition, there are also short comments on interesting points of technique, and simple descriptions of the derived structures that cannot be easily shown numerically. As some structures are too complex to be easily summarized in this manner, more detailed discussion can be found in Sec. 5.

Table 1 is organized so that a particular structure can be readily found. The entries are arranged with the following priorities:

1. Alphabetically by substrate.
2. Numerically by the surface plane Miller indices, i.e., (100) before (110) before (111).
3. Alphabetically by adsorbate, when present.
4. Size of the unit cell, i.e., (1×1) before (2×1) before (2×2). Here we arbitrarily assign $p(2\times2)$ higher priority than $c(2\times2)$.
5. Chronologically by date of publication.

Before are listed explanations of some of the symbols used as table headings and abbreviations and acronyms that may be encountered in the body of the tables. When an entry contains a dash (–), this indicates that this information was not specified. A query (?) indicates that the value of the parameter in question was discussed but not clearly defined.

1. Substrate:

The chemical symbol of the substrate.

2. Face:

The Miller indices of the surface under investigation.

3.Adsorbate:

The identity of any adsorbate present.

4. Symmetry:

The symmetry of the surface structure present, using standard notation.

5. Coverage:

The coverage of the surface by adsorbate in monolayers (ML).

6. Ref.:

The reference number of the study.

7. Method:

The method employed—SEXAFS or SEELFS.

8. Detection technique:

The manner in which the data were collected. The acronyms used are:

For SEXAFS studies:

ABS = absorption, AY = Auger yield, FY = fluorescence yield, PEXAFS = photoelectron EXAFS, PSID = photon stimulated ion desorption yield, PT = partial secondary electron yield, TY = total secondary electron yield.

For SEELFS studies:

CMA = cylindrical mirror analyzer, HG = hemispherical grid analyzer.

9. Analytical methods:

Other techniques that were used during the investigation to monitor surface composition or surface structure. Acronyms used here are:

AES = Auger electron spectroscopy, LEED = low-energy electron diffraction; PES = photoelectron spectroscopy.

10. Contamination level:

The reported level of surface contamination in monolayers, or other specified units. *L*(ow) indicates an unspecified "clean" state.

11. Flux:

The beam flux available in photons/s (SEXAFS) or μA (SEELFS).

12. Edge:

The absorption edge(s) investigated, using traditional x-ray notation—i.e., Pt L_2.

13. Energy range:

The fine-structure energy range in eV, either as given, or estimated from the data.

14. Angles:

The number of angles of incidence at which polarization data were taken.

15. Temperature:

The temperature at which the experiment was performed in degrees K.

16. Calculations:

The method of calculation used. Acronyms used are: SS = single shell analysis, MS = multiple shell analysis.

17. Reference compounds/phase shifts:

The compounds used for reference phase shifts, or the source, as a reference, of theoretical shifts.

18. Adsorption site:

The adsorption site symmetry, written as XF, meaning X-fold coordinate. Where ambiguity may exist, followed by symbols such as -*L* or -*S* to indicate long or short. See Sec. 5.2 for more details.

19. d(nn1):

The bond distance in Å to the first nearest-neighbor shell (*NN* 1) with error in parentheses when given.

20. nn1 pair:

The identities of the atoms involved in the first nearest neighbor shell.

21. d(nn2):

The bond distance in Å to the second nearest-neighbor shell (NN2) with error in parentheses when given.

22. nn2 pair:

The identities of the atoms involved in the second nearest-neighbor shell.

23. Comment:

Comments on any unusual aspects of the experiment or the reported structure.

TABLE 1. Surface structures determined by SEXAFS and SEELFS

Idx	Substrate	Face	Adsorbate	Symmetry	Coverage (ML)	Ref.	Method	Detection technique	Analytical methods	Contamn. level	Flux.
1	Ag	100	Cl	c(2×2)	0.5	27,28	SEXAFS	TY	LEED/AES	L	–
2	Ag	110	Cl	Incomm.	0.75	29	SEXAFS	TY	LEED/AES	L	–
3	Ag	110	O	(2×1)	–	30	SEXAFS	PY	LEED	–	–
4	Ag	111	Cl	$(\sqrt{3}\times\sqrt{3})$R30	0.66	27,31	SEXAFS	TY	LEED/AES	L	–
5	Ag	111	Cl	Disordered	0.33	31	SEXAFS	TY	LEED/AES	L	–
6	Ag	111	Cs	–	0.15	27,32	SEXAFS	TY	LEED/AES	L	5×E11
7	Ag	111	I	$(\sqrt{3}\times\sqrt{3})$R30	0.33	33	SEXAFS	AY	LEED/AES	?	1×E11
8	Ag	111	Pb	Incomm.	1	34	SEXAFS	FY	–	–	–
9	Al	100	–	(1×1)	–	35	SEXAFS	PY	AES	<.1% O	–
10	Al	111	–	(1×1)	–	35	SEXAFS	PY	AES	<.1% O	–
11	Al	111	O	(1×1)	<1	37	SEXAFS	TY	PES	–	–
12	Al	111	O	–	*	38	SEXAFS	PY/TY	LEED/AES	L	–
13	Al	Poly	O	–	1	39	SEXAFS	PEXAFS	–	–	–
14	Au	111	Ag	–	1	40	SEXAFS	FY	–	–	–
15	Au	111	Cu	–	1	36	SEXAFS	FY	–	–	–
16	B	Poly	–	–	–	41	SEELFS	CMA	AES	<5% N 3% C	2
17	C (g)	Poly	–	–	–	42	SEELFS	CMA	AES	<5% N, 3% C	2–20
18	C (g)	Poly	Br	–	0.2	43	SEXAFS	ABS	–	?	–
19	C (g)	Poly	Kr	$(\sqrt{3}\times\sqrt{3})$R30	0.35	44	SEXAFS	ABS	–	?	–
20	Co	11–10	C	(2×5)	0.3	45	SEELFS	CMA	LEED/AES	?	10–30
21	Cu	100	C_2H_2	–	–	47	SEXAFS	TY	–	–	–

Idx	Edge	E range (eV)	Angles	Temp. (K)	Calcs.	Ref. compds/ phase shifts	Adsorption site	d(nn1) (Å)	nn1	d(nn2) (Å)	nn2	Comments
1	Cl K	290	1	–	SS	AgCl	4F	2.69 (3)	Cl–Ag	–	–	Considered simple overlayer and mixed layer models. Simple overlayer gives best agreement.
2	Cl K	350	2	110	MS	AgCl	3F*	2.56 (4)	Cl–Ag	3.15 (4)	Cl–Cl	Considered mixed layer, fully incommensurate and vacancy domain wall models. Latter is best fit with distorted 3F site.
3	O K	250	3	–	SS	Ag_2O	2F(L)	2.06 (2)	O–Ag	2.17 (4)	O–Ag	2000 L O_2. O is 0.2 Å above surface.
4	Cl K	340	1	100	MS	AgCl	3F	2.80 (1)	Cl–Ag	2.93 (3)	Cl–Cl	Mixed layer model ruled out. Cl in 2/3 3F sites in graphitic arrangement.
5	Cl K	340	1	100	MS	AgCl	3F	2.70 (1)	Cl–Ag	3.95 (1)	Cl–Ag	Like 0.66 ML structure but with no Cl–Cl nn interactions.
6	Cs K	290	1	120	MS	CsBr, AgCl	–	3.20 (3)	Cs–Ag	–	–	Ionic bonding.
7	I L_3	230	1	110	SS	AgI	3F	2.87 (3)	I–Ag	–	–	
8	Pb L_3	400	1	300	SS	Pb, PbO_2	–	2.33 (2)	O–Pb	–	–	Epitaxial Ag on mica, electrochemically deposited Pb. Signal from Pb–O(?), not Pb–Ag due to incommensurate Pb overlayer.
9	Al L_{23}	35	1	–	*	–	–	?	Al–Al	–	–	Directly fitted bulk and surface EXAFS. Not relaxed.
10	Al L_{23}	35	1	–	*	–	–	2.81 (5)	Al–Al	–	–	Directly fitted bulk and surface EXAFS. Relaxed by 0.19 (0.06) Å.
11	O K	280	1	300	SS	Al_2O_3	3F	1.76 (5)	O–Al	–	–	50 L O_2/200 °C. Assumed 3F site. Al–O does not change up to 1 ML. Covalent bonding.
12	O K	300	2	–	SS	Al_2O_3	–	1.88 (3)	O–Al	–	–	1000 ML O_2/200 °C heat. O atoms penetrate Al to form oxide.
13	Al L_2	150	1	–	SS	[21]	3F	1.76 (4)	O–Al	3.00 (5)	Al–Al	25 L O_2. Oxygen penetrates; Al–Al distance increased from metal by 5%.
14	Ag K	400	1	300	SS	Ag_2O, Au–Ag	3F	2.42 (5)	O–Ag	2.75 (5)	Ag–Au	In-situ measurements on underpotentially deposited Ag on 2500 Å film Au on mica. Ag bound to H_2O or ClO_4^-.
15	Cu K	400	1	300	SS	CuO, Cu–Au	3F	2.08 (3)	O–Cu	2.5 (6)	Cu–Au	In-situ measurements on underpotentially deposited Cu on Au film on mica. Cu bound to oxygen, possibly in sulfate ion.
16	B K	300	1	300	SS	B, [21]	–	1.57 (8)	B–B	–	–	Phase shifts extrapolated from O and C and bulk B. B–B contracted relative to bulk (1.61 Å).
17	C K	200	1	300	SS	Diamond	–	1.38 (5)	C–C	–	–	
18	Br K	300	2	300	SS	Br_2	*	2.4 (1)	C–Br	2.24 (3)	Br–Br	*Br_2 physisorbed tilted by 42° in center of graphite ring.
19	Kr K	400	2	10,100	SS	Br_2, CBr_4	*	3.6 (1)	Kr–C	4.26 (5)	Kr·Kr	*Kr in center of graphite ring, coordination number not consistent with usual phase diagram.
20	C K	300	1	300	SS	[22,23]	3F	1.75 (5)	C–Co	–	–	Prefer model based on Co_2C with reconstructed hexagonal Co and C on top.
21	C K	300	1	60	MS	Cu phthalocyanin	μ_3*	1.42 (5)	C–C	1.87 (5)	C–Cu	Undissociated in μ_3 site (see text) 1.3 Å above Cu. Substrate assumed unreconstructed.

TABLE 1. Surface structures determined by SEXAFS and SEELFS – Continued

Idx	Substrate	Face	Adsorbate	Symmetry	Coverage (ML)	Ref.	Method	Detection technique	Analytical methods	Contamn. level	Flux.
22	Cu	100	C_2H_4	–	–	47	SEXAFS	TY	–	–	–
23	Cu	100	CH_3O	–	?	48	SEXAFS	PY	LEED/AES	L	–
24	Cu	100	Cl	c(2×2)	0.5	46	SEXAFS	AY	LEED	–	–
25	Cu	100	HCOO	–	?	49,50	SEXAFS	PY	LEED/AES	L	–
26	Cu	100	I	(2×2)	0.25	59	SEXAFS	TY	LEED/AES	L	–
27	Cu	100	O	c(2×2)	0.5	53	SEXAFS	PY	LEED/AES	L	–
28	Cu	100	Te	c(2×2)	0.25	54	SEXAFS	TY	LEED/AES	–	–
29	Cu	110	C	–	1	55	SEELFS	CMA	AES	<0.5%	2
30	Cu	110	HCOO	–	–	50,52,56	SEXAFS	PY	AES	–	–
31	Cu	110	I	c(2×2)	0.5	51	SEXAFS	AY	LEED/AES	–	1×E11
32	Cu	110	O	(2×1)	0.5	58	SEXAFS	PY	LEED/AES	L	–
33	Cu	111	Cl	$(\sqrt{3}\times\sqrt{3})$R30	0.33	57,60,61	SEXAFS	TY	LEED/AES /PED	L	–
34	Cu	111	Co	(1×1)	1	62,63	SEXAFS	TY	LEED/AES	–	–
35	Cu	111	I	$(\sqrt{3}\times\sqrt{3})$R30	0.33	51,59	SEXAFS	TY	LEED/AES	L	–
36	Cu	111	O	Disordered	0.5	64	SEXAFS	PY	–	–	–
37	Cu	111	Te	$(2\sqrt{3}\times\sqrt{3})$R30	0.33	54	SEXAFS	TY,AY	LEED/AES	–	–
38	Fe	110	O	–	0.6	65	SEELFS	–	AES	<3% C, N	5
39	Fe	Poly	C	–	–	66	SEELFS	CMA	AES	<0.5%	20
40	Fe	Poly	O	–	–	67	SEXAFS	TY	–	–	–
41	$Fe_{80}B_{20}$	Poly	–	–	–	41	SEELFS	CMA	AES	<5% N, 3%C	2
42	GaAs	110	O	–	1	68	SEXAFS	PY	PES	–	1×E9
43	Ge	111	Cl	(1×1)	1	69,70,102	SEXAFS	AY	LEED/AES	L	–
44	Ge	111	I	(1×1)	1	69,70,71	SEXAFS	TY,AY	LEED/AES	L	–
45	Ge	111	Te	(2×2)	0.5	69,70,71	SEXAFS	TY,AY	LEED/AES	L	–
46	InP	110	–	(1×1)	–	72,73	SEXAFS	PEXAFS	AES/PES	–	–

Idx	Edge	E range (eV)	Angles	Temp. (K)	Calcs.	Ref. compds/ phase shifts	Adsorption site	d(nn1) (Å)	nn1	d(nn2) (Å)	nn2	Comments
22	C K	300	1	60	MS	Cu phthalocyanin	4F*	1.47 (7)	C–C	1.86 (5)	C–Cu	Undissociated in symmetric site (see text) 1.25 Å above assumed nonreconstructed substrate.
23	O K	350	2	200	SS	Cu_2O	*	1.97 (5)	O–Cu	–	–	* Top site ruled out, C–O bond tilted about 30°. 30 L O_2 + satn. CH_3OH annealed at 300 K.
24	Cl K	450	2	–	SS	CuCl	4F	2.37 (2)	Cl–Cu	–	–	15 L Cl_2/room temp then 100 °C for 2 min.
25	O K	260	2	200	MS	–	1F	2.0 (1)	O–Cu	–	–	Used data from [115], but place formate diagonally on on-top site. See text.
26	I L_3	300	2	–	SS	CuI	4F	2.69 (2)	I–Cu	–	–	
27	O K	350	2	–	SS	Cu_2O	4F	1.94 (4)	O–Cu	–	–	300 L O_2, no annealing.
28	Te L_3	230	2	300	SS	Cu_2Te	4F	2.62 (4)	Te–Cu	–	–	Te vapor, annealed 350 °C/5 min.
29	C K	250	1	300	*	[21]	–	1.47	C–C	–	–	* Direct fitting of RDF. C from CO. Graphitic C layer 1.27 Å above Cu, long C–C bond.
30	O K	120	4	300	SS	–	1F	1.98 (7)	O–Cu	1.25 (5)	C–O	Used NEXAFS data as well. 10 L HCOOH/300 K. C in 1F site on ridge, O near 2F–L.
31	I L_3	–	2	110	SS	CuI	–	–	–	–	–	Molecular I_2 after 400 °C anneal; atomic I at higher annealing temperatures.
32	O K	380	3	–	SS	Cu_2O	2F(L)	1.84 (2)	O–Cu	1.99 (2)	O–Cu	Update of [116]. Substrate reconstructed with missing rows. See text.
33	Cl K	350	2	–	SS/MS	CuCl	3F	2.39 (2)	Cl–Cu	–	–	PED resolved fcc type of 3F site.
34	Co K	400	2	–	SS	[21,24]	3F	2.51 (3)	Co–Cu	2.51 (3)	Co–Co	
35	I L_3	300	2	–	SS	CuI	3F	2.66 (3)	I–Cu	–	–	
36	O K	370	3	–	–	–	3F	1.83 (2)	O–Cu	3.1 (1)	Cu–Cu	1800 L O_2. O not incorporated, within 0.2 Å of Cu. Substrate reconstructed Cu–Cu distance close to Cu_2O
37	Te L_3	230	2	300	SS	Cu_2Te	*	2.69 (4)	Te–Cu	–	–	Te vapor, annealed 350 °C/5 min. * substitutional displacement of Cu atoms by Te
38	Fe M_{23}	–	1	300	SS	*	2F(L)	1.95 (5)	O–Fe	2.65	Fe–Fe	6 L O_2. 7% expansion of Fe top layer spacing. At 100 L O_2, reconstruction to FeO(111)-type structure (?).
39	C K, Fe M_{23}	140	1	–	SS	Fe_3C	–	–	–	–	–	C from CO at <200 °C. Fe_3C-like structure, C in trigonal prism of 6 Fe.
40	Fe K	350	1	300	SS	[21]	–	2.04	O–Fe	–	–	Natural oxide of ferritic Fe.
41	B K	300	1	300	SS	B, [21]	–	2.14	Fe–B	–	–	Phase shifts extrapolated from O and C and from bulk B. Also measured $Fe_{78}Si_5B_{17}$.
42	O K	270	1	300	SS	NiO	–	1.70 (5)*	–	–	–	6×E9 L O_2. Atomic O on surface. * Bond length uncertain because of phase shift difficulties.
43	Cl K	300	1	300	SS	$GeCl_4$	1F	2.07 (3)	Cl–Ge	–	–	Disagreement with photoemission data.
44	I L_3	220	3	300	SS	GeI_4	1F	2.50 (4)	I–Ge	4.06 (5)	–	Annealed 400 °C/5 min.
45	Te L_3	220	3	300	SS	GeI_4	3F	2.7	Te–Ge	–	–	Annealed 400 °C/5 min.
46	P L_2	110	1	–	SS	[21,23]	–	2.43 (4)	P–In	4.06 (5)	P–P	Prepared by cleavage. Contraction in vertical and horizontal dimension.

TABLE 1. Surface structures determined by SEXAFS and SEELFS – Continued

Idx	Substrate	Face	Adsorbate	Symmetry	Coverage (ML)	Ref.	Method	Detection technique	Analytical methods	Contamn. level	Flux.
47	InP	110	Al	–	*	72	SEXAFS	PEXAFS	AES/PES	–	–
48	InP	110	Na	–	0.12	74	SEXAFS	PEXAFS	AES/PES	–	–
49	MgO	100	–	(1×1)	–	75	SEELFS	CMA	AES	L	–
50	Mo	100	O	–	–	76	SEXAFS	PSID	–	L	–
51	Ni	100	Br	c(2×2)	0.5	77	SEXAFS	FY	LEED/AES	–	1×E8
52	Ni	100	C	(2×2)p4g	0.25	80	SEXAFS	PY	–	–	–
53	Ni	100	C	?	–	79	SEELFS	–	AES/XPS	L	–
54	Ni	100	C_4H_4S	c(2×2)	–	81	SEXAFS	FY,AY	–	–	2×E10
55	Ni	100	I	–	1	82	SEXAFS	TY	LEED/AES	L	–
56	Ni	100	I	c(2×2)	0.5	83,84	SEXAFS	TY	LEED/AES	L	–
57	Ni	100	N	(2×2)p4g	0.25	85,86	SEXAFS	PY	?	?	5×E10
58	Ni	100	O	(2×2)	0.25	87	SEXAFS	PY	LEED/AES	<1% C,O	–
59	Ni	100	O	c(2×2)	0.5	88	SEELFS	CMA	LEED/AES	<1%	5
60	Ni	100	S	c(2×2)	0.5	89	SEXAFS	FY	LEED/AES	–	–
61	Ni	110	C	–	–	91	SEELFS	CMA	AES	<1%	2
62	Ni	110	O	(2×1)	0.33	92,93	SEXAFS	PY	LEED	–	–
63	Ni	110	S	c(2×2)	0.5	94,95	SEXAFS	AY	LEED/AES	<3% C,S	–
64	Ni	111	C	(1×1)	–	96	SEELFS	CMA	LEED/AES	<1%	5
65	Ni	111	S	(2×2)	0.25	94	SEXAFS	AY	LEED/AES	<3% C,S	–
66	Ni	111	S	(5×5)	–	94	SEXAFS	AY	LEED/AES	<3% C,S	–
67	Si	100	H_2O	(2×1)	0.5	97	SEXAFS	PSID	LEED/AES	L	–
68	Si	100	K	(2×1)	0.5	98	SEXAFS	TY,AY	LEED/AES	L	–

Idx	Edge	E range (eV)	Angles	Temp. (K)	Calcs.	Ref. compds/ phase shifts	Adsorption site	d(nn1) (Å)	nn1	d(nn2) (Å)	nn2	Comments
47	P L_2	110	1	300	SS	[21,23]	–	2.94 (4)	P–In	4.13 (5)	P–P	1 Å Al by evaporation, removes relaxation. Al in clusters and not located.
48	P L_2	120	1	300	SS	[21,23]	–	2.49 (4)	In–P	4.17 (9)	P–P	Clean surface reconstruction removed and new 3.15 Å P–In distance.
49	O K	90	1	300	MS	–	–	2.2	O–Mg	3.04	O–O	Cleaved sample. Inward relaxation of 17% with O atom 2.2 Å above MgO.
50	Mo L_1	550	1	–	SS	–	–	–	–	–	–	100 L O_2. No reconstruction of Mo; cannot distinguish Mo–O from Mo–Mo.
51	Br K	250	1	300	SS	$NiBr_2$	4F*	2.32 (4)	Br–Ni	–	–	50 L Br_2/670 K. *Amplitudes consistent with 4F site.
52	C K	150	2	300	SS	?	4F	1.82 (5)	C–Ni	2.9 *	–	40 L C_2H_4/500 K. Ruled out "4F bridge" site, favor 4F hollow with C 0.1 Å above reconstructed Ni. *Cannot fit.
53	C K	200	1	–	SS	[21]	–	1.75 (5)	C–Ni	–	–	5400 L CO/380 K. Compared with cluster calcn. Carbidic C 0.1 Å above plane.
54	S K	260	2	100	SS	–	4F	2.22 (2)	S–Ni	–	–	Looks similar to H_2S. Thiophene appears to dissociate even at 100 K.
55	I L_3	250	1	300	SS/MS	NiI_2	*	2.78 (3)	I–Ni	–	–	*Surface NiI_2 iodide phase formed by cooling from 350 K in I_2 vapor.
56	I L_3	250	2	300	SS/MS	NiI_2	4F	2.78 (2)	I–Ni	–	–	Also discusses 2 lower coverage phases and surface iodide phase.
57	N K	250	2	90,295	SS/MS	NiO	4F	1.89 (3)	N–Ni	2.72 (5)	Ni–Ni	N atom is 0.11(6) Å above Ni plane. Ni atoms rotated by tangential displacement of 0.77 Å.
58	O K	220	1	–	SS	NiO	4F	1.96 (3)	O–Ni	–	–	1.5 L O_2. O is 0.86(7) Å above Ni plane.
59	O K, Ni M_{23}	160	1	300	SS	NiO	4F	1.96 (5)	O–Ni	–	–	At high coverages islands of NiO form.
60	S K	350	2	95	SS	–	4F	2.22 (3)	S–Ni	–	–	Used NEXAFS, some disagreement with previous HREELS results. See text.
61	C K, Ni L_{23}	100	1	–	MS	[21]	–	1.49	C–C	1.95	C–Ni	1000's L CO/600 K. Graphitic C with strong interaction with substrate; in registry along [110].
62	O K	250	4	–	SS	NiO	2F(L)	1.85 (3)	O–Ni	1.96 (8)	O–Ni	0.8 L O_2/190 °C. Supports sawtooth model, O tilted towards (100) by 20° and 0.56 Å above Ni (see text).
63	S K	220	3	300	MS	NiS	4F	2.23 (4)	S–Ni	2.31 (2)	S–Ni	8 L H_2S/120 °C. S in rectangular 4F site, bonded to 2nd layer atoms. First substrate spacing decreased by 12%.
64	C K	220	1	–	MS	[21]	3F*	1.45 (3)	C–C	2.50 (3)	C–C	300 L CO/300 °C. Graphitic C 2.8 Å above Ni and in registry, substrate not reconstructed. C–C slightly expanded.
65	S K	320	2	150,293	MS	NiS	3F	2.23 (2)	S–Ni	3.35 (3)	?	6 L H_2S/200 K.
66	S K	320	2	150,293	MS	NiS	3F?	2.27 (2)	S–Ni	–	–	5 L H_2S/450 K. Data could favor 3F or 4F site.
67	Si K	220	1	300	MS	Si	*	2.37 (2)	Si–Si	3.90 (15)	Si–Si	1 L H_2O/290 K. * Consistent with symmetric and asymmetric dimer models (see text).
68	K K	170	2	120–300	SS	Si	*	3.14 (10)	K–Si	–	–	*Consistent with 1-D K chains along (110) and weak bonding to Si.

TABLE 1. Surface structures determined by SEXAFS and SEELFS – Continued

Idx	Substrate	Face	Adsorbate	Symmetry	Coverage (ML)	Ref.	Method	Detection technique	Analytical methods	Contamn. level	Flux.
69	Si	100	O	(1×1)	2–3	99	SEXAFS	TY	LEED/AES	L	–
70	Si	100	O	–	–	100	SEXAFS	PY	–	–	1×E12
71	Si	111	Ag	$(\sqrt{3}\times\sqrt{3})$R30	0.66	101	SEXAFS	AY	LEED	L	5×E10
72	Si	111	Ag	(1×1)	>1	101	SEXAFS	AY	LEED	L	5×E10
73	Si	111	Ag	(7×7)	0.33	101	SEXAFS	AY	LEED	L	5×E10
74	Si	111	Cl	(7×7)	1	69,70,102	SEXAFS	AY	LEED/AES	L	–
75	Si	111	Co	–	–	103	SEXAFS	TY	LEED/AES	–	–
76	Si	111	Ge	(7×7)	1	104	SEXAFS	TY	LEED/AES	L	–
77	Si	111	I	(7×7)	1	69,70,71	SEXAFS	TY,AY	LEED/AES	L	–
78	Si	111	N	(8×8)	?	105	SEELFS	CMA	LEED/AES	L	3–10
79	Si	111	Ni	?	0.5	106	SEXAFS	AY	LEED/AES	–	–
80	Si	111	O	–	?	107	SEXAFS	TY	–	–	1×E9
81	Si	111	Pd	(7×7)	1.5	101b	SEXAFS	AY	LEED	?	1×E10
82	Si	111	Pt	(7×7)	0.8	108,109	SEXAFS	TY	LEED/AES	L	–
83	Si	111	Te	(7×7)	1	69,70,71	SEXAFS	TY,AY	LEED/AES	L	–
84	Si	Poly	Ti	–	>1	110	SEELFS	HG	LEED/AES	–	–
85	W	Poly	Ba,O	–	–	111,112	SEXAFS	TY	AES	L	–
86	ZnO	Poly	–	–	–	114	SEELFS	CMA	–	–	–

Idx	Edge	E range (eV)	Angles	Temp. (K)	Calcs.	Ref. compds/ phase shifts	Adsorption site	d(nn1) (Å)	nn1	d(nn2) (Å)	nn2	Comments
69	O K	280	2	300	SS	SiO_2	2F	1.65 (2)	O–Si	–	–	O atoms occupy 2 types of bridge sites, between Si atoms in asymm. dimer top layer, and between atoms in different layers.
70	O K	350	1	300	SS	SiO_2	–	1.61 (2)	O–Si	–	–	Used native oxide and clean wafer exposed to O_2. Si–O distance as in α-quartz.
71	Ag L_2	–	3	300	SS	Ag, InP	3F*	2.48 (4)	Ag–Si	–	–	Ag/Si(7×7)/200–600 °C anneal. Ag atoms embedded in Si in 3F site 0.7 Å below top Si layer.
72	Ag L_2	–	3	300	SS	Ag, InP	*	2.86 (3)	Ag–Ag	–	–	Ag on Si(7×7). Ag metal islands form.
73	Ag L_2	–	3	300	SS	Ag, InP	3F	2.48 (5)	Ag–Si	–	–	Ag on Si(7×7) 300 K. Ag in 3F site 0.7 Å above Si outer layer; some Si lateral movements.
74	Cl K	300	2	300	SS	$SiCl_4$	1F	2.03 (3)	Cl–Si	3.51 (6)	Si–Si	Similar results for adsorption on the quenched $(\sqrt{19}\times\sqrt{19})$ structure.
75	Co K	300	2	300	SS	$CoSi_2$	8F	2.35 (3)	Co–Si	–	–	Very thin layer of $CoSi_2$ with Si on top leading to 8F Co coordination at interface. Contracted 2.5% perpendicularly.
76	Ge K	300	1	300	SS	Ge, Ge–Si	3F	2.30 (2)	Ge–Si	2.44 (2)	Ge–Ge	Strain of Ge-Si bond angle leads to Ge chains parallel to surface (see text).
77	I L_3	220	3	300	SS	$SiI(CH_3)_3$	1F	2.44 (3)	I–Si	–	–	Annealed 400 °C/5 min.
78	N K	240	1	300	SS	[21]	?	1.54 (4)	N–Si	–	–	2400 L N_2/W filament/850 °C. N not in 3F site, possibly bridge site. Also studied higher temperature "quadruplet" structure.
79	Ni K	350	1	300	SS	$NiSi_2$, NiSi	6F	2.37 (3)	Ni–Si	–	–	Ni is hollow between 1st and 2nd layers of Si; Si expanded outwards by 0.8 Å. At higher coverages Ni substitutes for Si.
80	O K	220	1	300	SS	SiO_2	–	1.65	O–Si	–	–	1×E6 L O_2 on cleaved sample. Several models discussed.
81	Pd L_2	150	1	300	SS	Pd_2Si	–	?	Pd–Si	?	Pd–Pd	1.5 ML Pd. Compound formation resembling Pd_2Si. See text.
82	Pt L_3	300	1	300	MS	PtSi	6F	2.48 (3)	Pt–Si	3.81 (5)	Pt–Si	Pt in interstitial Si sites, expanding Si lattice. More Pt leads to formation of Pt_2Si.
83	Te L_3	220	3	300	SS	$SiI(CH_3)_3$	2F	2.47 (3)	Te–Si	–	–	
84	Ti L_{23}	250	1	300	SS	[21]	–	2.39 (4)	Ti–Si	–	–	Ti evaporated and annealed 400 °C for silicide phase.
85	Ba L_3	220	1	300,1100	MS	BaO	4F	2.62 (4)	O–Ba	3.59 (12)	Ba–W	Thermionic cathodes. Ba and BaO at surface with Ba coordinated directly to O. Also measured W–Os and W–Pt. See text.
86	Zn M_{23}	260	1	300	SS	[21]	–	2.02 (1)	O–Zn	–	–	Zn–O 0.02 Å larger than in bulk ZnO.

5. Discussion of Structural Results

5.1. Metal Systems

Due to the difficulty in separating bulk and surface signals, fine-structure spectroscopies have found little utility in probing the crystallography of clean metal surfaces. One attempt to fit directly bulk and surface SEXAFS data from Al(100)[35] found no evidence for relaxations at the surface. The energy range of the dataset used for this study was extremely short, only about 35 eV, and it is possible that the agreement with LEED studies[117,118] in finding no surface relaxations is fortuitous. A number of SEELFS studies[12,13] have made measurements of signals from clean metal surfaces, but have not reported surface bond lengths. One study of Fe–B alloys reported apparent surface Fe–B bond lengths.[41]

5.1.a. Atomic Adsorbates

One of the areas in which the capabilities of extended fine-structure techniques have been most thoroughly exploited is in atomic adsorption. In common with the general trend observed in surface structural studies, such adsorbates have been found to tend to occupy high-symmetry sites on the surface. For the convenience of the reader Fig. 1 illustrates some typical examples of such adsorption sites for low-index surfaces.

In the early days of SEXAFS the best signal strengths could be obtained for a high-Z atomic adsorbate, such as I, adsorbed on a first- or second-row transition metal. As a result there are a substantial number of such SEXAFS studies involving halogen adsorbates to be found in the literature. Relatively few of these systems have been studied by other

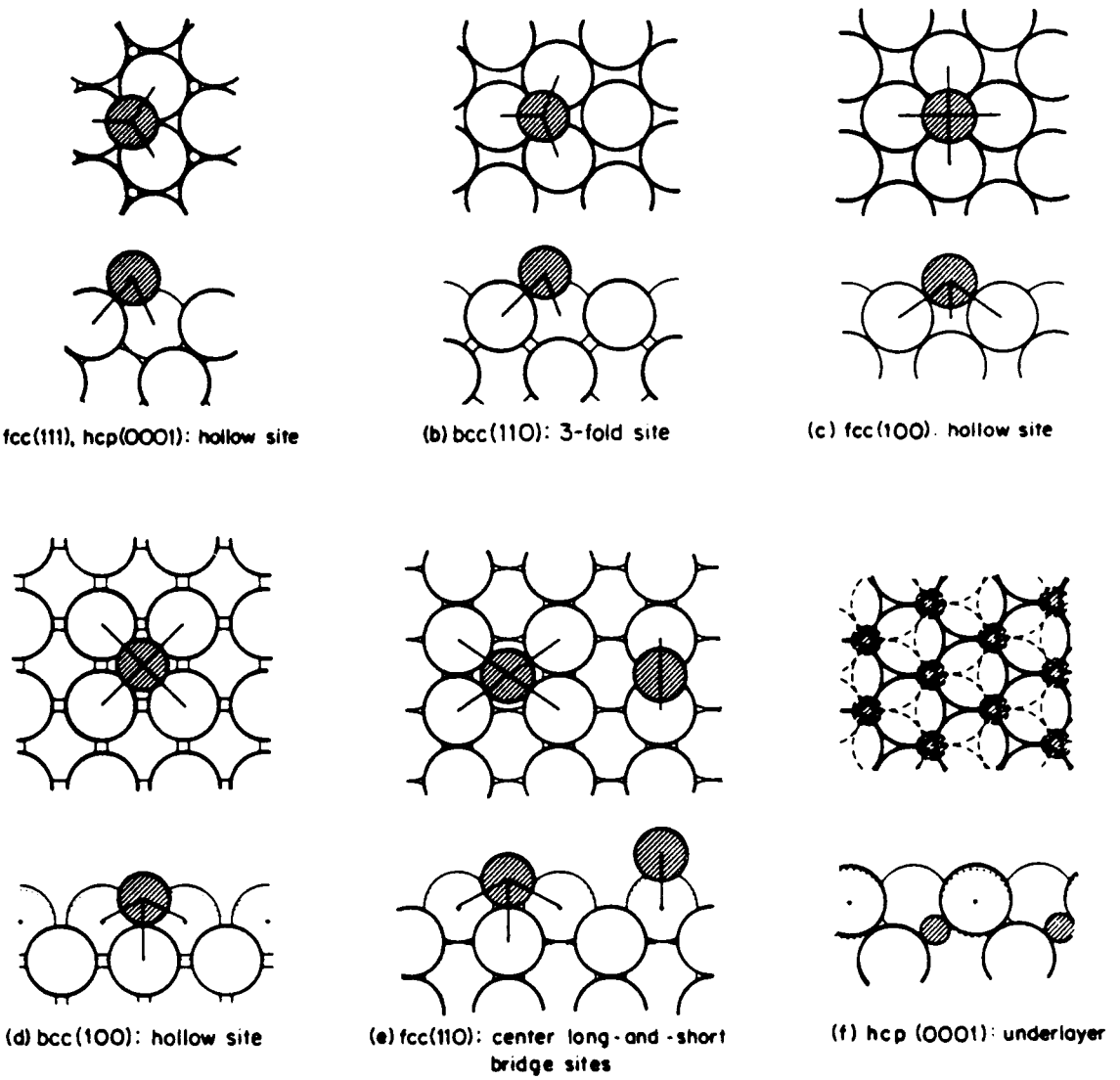

FIG. 1. Schematic diagram (top and side views) of high-symmetry atomic adsorption sites (adsorbates shown shaded) on low-index metal surfaces. Reprinted with permission of Springer [G. A. Somorjai and M. A. Van Hove, *Adsorbed Monolayers on Surfaces* (Springer-Verlag, Berlin, 1981), Fig. 6.2].

TABLE 2. Surface bond lengths (d) from SEXAFS investigations compared with results from other techniques for atomic halogen adsorbates on fcc metal surfaces.

Surface	Adsorbate	Symmetry	Site	d(Å)	Method	Ref.
Ag(100)	Cl	$c(2\times2)$	$4F$	2.69	SEXAFS	27,28
			$4F$	2.61	LEED	119,120
(110)	Cl	Incomm.	$3F$[a]	2.56	SEXAFS	29
(111)	Cl	Disordered[b]	$3F$	2.70	SEXAFS	27,31
		$(\sqrt{3}\times\sqrt{3})R\,30$[c]	$3F$	2.70	SEXAFS	31
	I	$(\sqrt{3}\times\sqrt{3})R\,30$	$3F$	2.87	SEXAFS	33
			$3F$	2.83	LEED	122
Cu(100)	Cl	$c(2\times2)$	$4F$	2.37	SEXAFS	46
			$4F$	2.41	LEED	123
	I	(2×2)	$4F$	2.69	SEXAFS	59
(111)	Cl	$(\sqrt{3}\times\sqrt{3})R\,30$	$3F$	2.39	SEXAFS	57,60,61
	I	$(\sqrt{3}\times\sqrt{3})R\,30$	$3F$	2.66	SEXAFS	51,59
Ni(100)	Br	$c(2\times2)$	$4F$	2.32	SEXAFS	77
	I	$c(2\times2)$	$4F$	2.78	SEXAFS	82–84

[a] 0.75 ML coverage; distorted $3F$ site.
[b] 0.33 ML coverage.
[c] 0.66 ML coverage.

surface structural techniques; a comparison of the available data is presented in Table 2.

We can see from Table 2 that in those cases where LEED data are available in addition to SEXAFS the level of agreement on the identity of the adsorption site and the bond length is generally good. The $4F$ site on the (100) surface of the face-centered cubic (fcc) metals Ag, Cu, and Ni is always preferred. The case of Cl/Ag(100) is, however, instructive. The $c(2\times2)$ 0.5 ML coverage structure of Cl on Ag(100) has been the subject of several investigations. An early LEED study[119] found reasonable agreement with a mixed Ag–Cl surface layer model, but best agreement with a simple overlayer $4F$ hollow structure at an Ag–Cl bond distance of 2.67 Å. This figure was later reanalyzed[120] to a revised value of 2.61 Å. The first SEXAFS investigation on this system[121] was unable to obtain good quality data, and deduced a Cl–Ag distance of 2.53 Å from their previous result on Cl/Cu(100),[46] by assuming a surface radius of 1.09 Å for Cl. Later SEXAFS work[27,28] produced analyzable data that indicated a $4F$ site with an Ag–Cl bond length of 2.69 Å, in reasonable agreement with the LEED figures.

Investigations of halogen adsorption on the (111) surfaces of these metals center on the frequently observed $(\sqrt{3}\times\sqrt{3})R\,30°$ symmetry LEED pattern, usually found at 1/3 ML coverage. In most cases the assignments have been relatively straightforward implicating the $3F$ site. On fcc(111) surfaces, there are in fact two slightly inequivalent $3F$ adsorption sites, one in the "expected" continuation of the fcc stacking sequence, and a second in the hexagonal close-packed (hcp) site where there is an atom in the second substrate layer directly beneath the adsorbate. Such subtle distinctions are difficult to observe by any surface structural technique; in one case—that of Cl/Cu(111)[57]—while SEXAFS alone data could not distinguish between the two types of $3F$ sites, additional photoelectron diffraction data placed the Cl atom in the fcc $3F$ site.

In the case of Cl/Ag(111),[27,31] Lamble *et al.* found that the $(\sqrt{3}\times\sqrt{3})R\,30°$ symmetry LEED pattern occurred at a coverage of 2/3 ML, rather than the expected 1/3 ML, and that at the lower coverage the LEED pattern was too diffuse to characterize, indicating a disordered overlayer. They were able using a multishell approach to derive the same bond length of 2.70 Å and a $3F$ adsorption site for both coverages. The multishell calculation also allowed the derivation of several intershell distances shown in Table 3. The proposed structure for 2/3 coverage, depicted in Fig. 2, consists of a vacancy honeycomb, or graphitic, arrangement of Cl atoms in 2/3 of the available $3F$ sites. The presence of neighboring Cl atoms at a distance of 2.93 Å is apparent in this structure. At a Cl coverage of 1/3, the radial distribution peak corresponding to this distance disappears. A normal ordered 1/3 ML $(\sqrt{3}\times\sqrt{3})R\,30°$ structure is recovered from this model by removing every third Cl atom, marked A in Fig. 2, thereby avoiding any nearest-neighbor 2.93 Å interactions. Presumably at this coverage for this system, the Cl–Ag interactions are sufficiently weak to prevent ordering. The authors emphasize that this structure comes directly from the experimental data via a multishell calculation, and is not an input to the calculation. This is in contrast to LEED

TABLE 3. Bond distance (Å) from SEXAFS measurements on the Cl/Ag(111) system at 1/3 and 2/3 ML coverage.[27,31]

Shell	Bond distance (Å) 1/3 ML	2/3 ML
Cl–Ag	2.70 ± 0.01	2.70 ± 0.01
Cl–Cl	···	2.93 ± 0.03
Cl–Ag	3.68 ± 0.06	3.71 ± 0.1
Cl–Cl	5.14 ± 0.20	4.83 ± 0.2

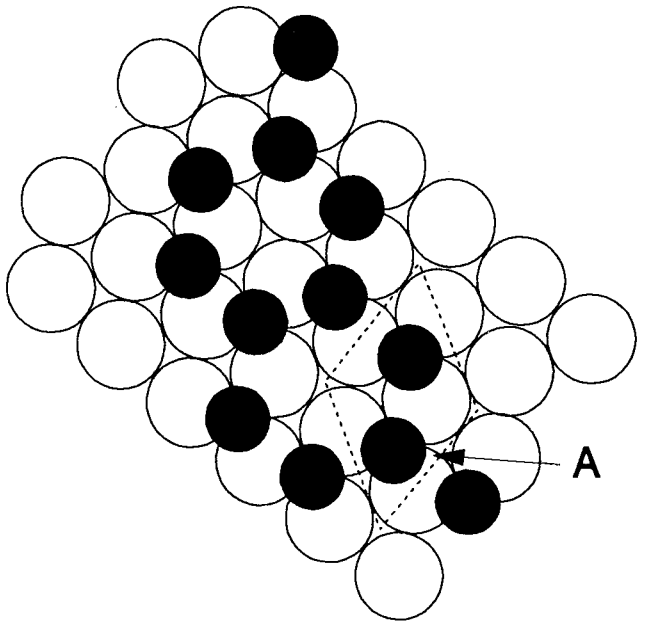

FIG. 2. The vacancy honeycomb structure proposed for the 2/3 ML $(\sqrt{3}\times\sqrt{3})R\,30°$ Cl/Ag(111) system, showing the unit mesh. Removing the atom marked A and its symmetric equivalents produces an ordered 1/3 ML structure. Adapted from Ref. 31.

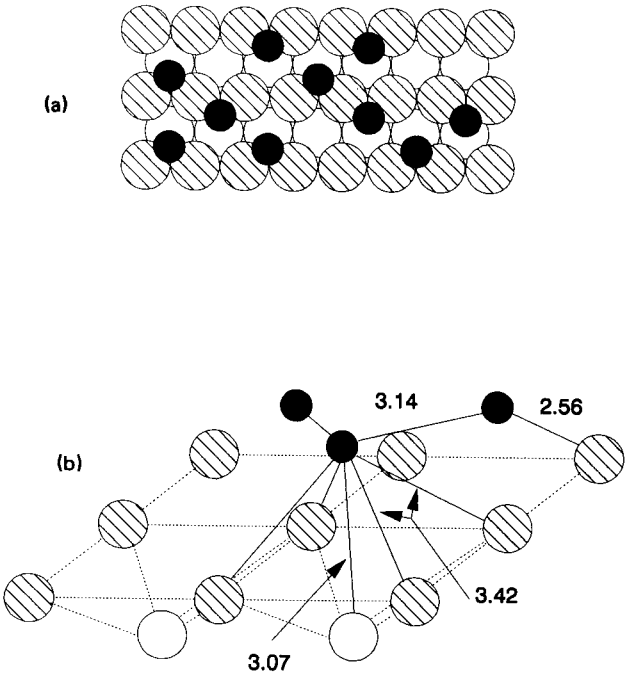

FIG. 3. (a) Plan view of vacancy domain wall model for the incommensurate 0.75 ML Cl/Ag(110) system. Cl atoms (filled) occupy pseudothreefold (B_3) sites—both Cl–Ag bonding radii and Cl–Cl repulsive radii are shown. Silver atoms are shaded (top-layer) or unfilled (second layer). (b) Isometric projection. Adapted from Ref. 29.

experiments, where the process is one of trial-and-error fitting of postulated structures. In any case, the lower coverage structure could not have been tackled using conventional LEED because of the diffuse nature of the LEED pattern. This observation underscores the usefulness of the short-range nature of the SEXAFS experiment for weakly ordered systems. However, we should note that the new technique of diffuse LEED[124] could be used in this situation.

The only SEXAFS study of halogen adsorption on the (110) surface of an fcc metal—Cl/Ag(110) by King and coworkers[29]—has some unusual features. The Ag–Cl nearest-neighbor distance of 2.56 Å is considerably shorter than that observed on either the (111) or (100) surfaces, and is independent of coverage. At 0.75 ML coverage an incommensurate structure forms, which has been previously interpreted in terms of a mixed layer[125] or a fully incommensurate overlayer.[126] The SEXAFS-derived (multishell analysis) Cl–Cl bond length of 3.14 Å is much too short to fit either of these models. A vacancy domain wall structure, shown in Fig. 3, is consistent with the SEXAFS and LEED data; here the Cl atoms are positioned in distorted out-of-plane pseudothreefold sites, essentially a $2F$-L site tipped toward the center of the rectangular substrate unit cell.

An important aspect of atomic adsorption (that appears to be becoming increasing common as structural investigations become more detailed and accurate) is that adsorption can often lead to rearrangement of the substrate atoms. Such rearrangements can involve a relatively subtle effect such as vertical displacements of atoms to produce a relaxation or rumpling of the spacings between atomic planes, or possibly act to relieve one already in existence in the clean surface. Other modes of surface rearrangement may range from small lateral movements of atoms within a surface plane, to wholesale mass transport of rows of atoms to produce dramatic reconstructions.

The halogen systems listed in Table 2 all appear to be simple overlayer structures with no substrate reconstruction. However, many of these investigations predated the discovery of the prevalence of adsorption-induced relaxations and reconstructions. As a result such rearrangements were not usually considered in formulating the structural models considered in these studies. It is possible that some of these studies could be profitably reexamined with the possible presence of such substrate modifications in mind.

A second class of adsorbates that has been quite extensively studied by the SEXAFS community are the chalcogens, particularly oxygen and sulfur. In these cases a number of adsorbate-induced substrate reconstructions have been reported by other techniques and incorporated into the SEXAFS investigations. The cases of O and S adsorbed on the (100) and (110) surfaces of Ni and Cu are instructive in this regard, and are summarized in Table 4.

The ordered $p(2\times2)$ and $c(2\times2)$ O and S overlayers on Ni(100) have long been considered to be a prime example of a simple, well-understood adsorption system. In the case of the sulfur adlayer, the $4F$ site and bond length from SEXAFS[89] are in good agreement with LEED[137] and low-energy ion-scattering data.[141] Early LEED,[136,137] ion-scattering,[139,140] SEXAFS,[87] and SEELFS[88] studies all placed the O atom in a $4F$ site with a bond length of 1.96 ± 0.04 Å. The most recent SEXAFS[81,86] experiments with better sig-

TABLE 4. Surface crystallographies from SEXAFS investigations compared with results from other techniques for O and S adsorbed on low index faces of Cu and Ni.

Surface	Ads. atom	Symmetry	Site	Bond length d(Å)	Substrate reconstr.[a]	Method	Ref.
Cu(100)	O	$c(2\times2)$	$4F$	1.94	**	SEXAFS	53
		$(2\sqrt{2}\times\sqrt{2})R45$	pseudo-$4F$	1.91	MR	LEED/EELS	127,128
		$c(2\times2)$	$2F/4F$	···	None	LEIS	129,130
(110)	O	(2×1)	$2F$-L	1.84,2.00	MR	SEXAFS	58
				1.81,1.98	MR	LEED	131
Ni(100)	O	$c(2\times2)$	$4F$	1.96	**	SEXAFS	85–87
				1.98	**	LEED	136.137
				1.92	**[b]	LEED	138
				1.97	**	LEIS	139
				1.88	??	MEIS	140
	S	$c(2\times2)$	$4F$	2.22	**	SEXAFS	89
				2.19	**	LEED	137
				2.35	**	LEIS	141
(110)	O	(2×1)	$2F$-L	1.85	ST	SEXAFS	92,93
				···	ST	MEIS,STM	144,145
				1.77	MR	LEED	143
				1.80	MR	MEIS,LEIS	146,147
	S	$c(2\times2)$	pseudo-$4F$	2.23	**	SEXAFS	94,95
				···	**[b]	LEED	148
				···	??	LEIS	141
				2.32	**	MEIS	149

[a] ** = not investigated; MR = missing row; ST = sawtooth; ?? = possible reconstruction.
[b] Some relaxation and rumpling of substrate.

nal-to-noise again produce the same bond length and rule out an symmetric "off-center" $4F$ site[150] due to the lack of a beating effect in the SEXAFS amplitudes between 3–5 Å.

Because of the unanimity in these results and the apparent simplicity of the system, there has been little or no attempt to include substrate rearrangements in the models proposed for the O/Ni(100) system. However, a recent LEED study[138] (Oed *et al.*) to be published for the $c(2\times2)$ phase, indicates that even in such an apparently well-characterized simple system some degree of relaxation or reconstruction may be occurring. Their results are in agreement with the established structure in the identity of the adsorption site and the bond length. However, the best fit to the new LEED data are for a change in the first interlayer spacing d_{12} from a 1% contraction seen with the clean Ni(100) surface to a 6% expansion, in good agreement with previous ion scattering results,[140] together with a small buckling of the second metal layer as shown in Fig. 4.

While these substrate rearrangements observed by LEED are not large they do lead to some interesting conclusions. Oed *et al.*[138] note that inclusion of these substrate effects leads to a Ni–O interlayer distance d_0 of 0.77 Å, whereas fixing the first Ni–Ni spacing d_{12} at the bulk value, rather than at a + 6% expansion, results in a much larger oxygen

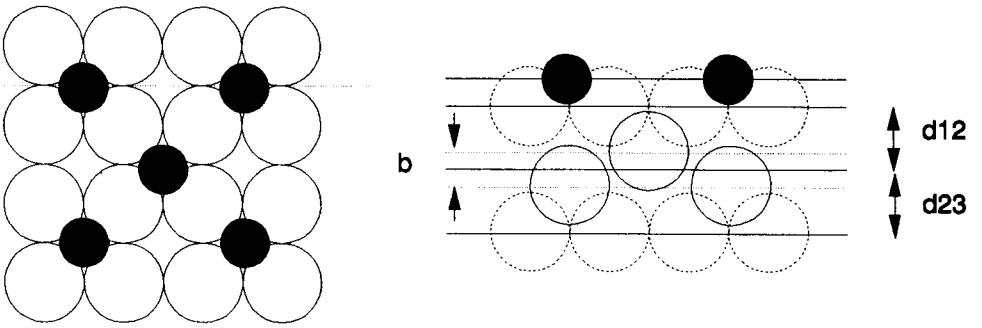

FIG. 4. Structure proposed[138] for the $c(2\times2)$ O/Ni(100) system including relaxation and buckling in the substrate.

layer separation of $d_0 = 0.85$ Å. This is the same value found in previous LEED and SEXAFS investigations that did not allow for any substrate rearrangements. At the same time these subtle rearrangements do not change the nearest-neighbor Ni–O bond length, only the interplanar distances! The lesson that we might draw from this is that determining just the first adsorbate–substrate shell distance from a SEXAFS study is often not sufficient to distinguish adsorbate-induced changes in the substrate. The SEXAFS study of Arvanitis *et al.*[86] only found the first-shell spacing from a single-shell analysis; it might be interesting to perform a full multishell analysis on these data to see if the substrate relaxations shown in Fig. 4 can be confirmed.

In contrast, structural analyses of the analogous O/Cu(100) system have been plagued with difficulties from the beginning. A number of chemisorption phases have been reported, the two most important being the $(\sqrt{2}\times\sqrt{2})R\,45°$, known more simply in Wood notation as $c(2\times2)$, and the $(2\sqrt{2}\times\sqrt{2})R\,45°$. These are often reported as forming sequentially with increasing O coverage, prior to the onset of bulk oxide formation.[151] Alternatively, some authors[152] view the $(2\sqrt{2}\times\sqrt{2})R\,45°$ phase as the truly stable phase and believe that the $c(2\times2)$ LEED patterns are only observed when the ordering of the adsorbate is insufficient to provide measurable intensities for the 1/4 order beams.

The sole SEXAFS study by Doebler *et al.*[53] for this system used a low O_2 exposure and no annealing to attempt to generate a true $c(2\times2)$ structure. The polarization-dependent amplitude ratios that they found are only consistent with adsorption in a 4*F* hollow site and a single scattering analysis gave a Cu–O bond length of 1.94 Å. The most recent LEED[127] and high-resolution electron energy loss spectroscopy (HREELS)[128] studies of the $(2\sqrt{2}\times\sqrt{2})R\,45°$ phase yield a nearest-neighbor Cu–O bond length of 1.91 Å in good agreement with the SEXAFS result. However, these new studies also show that only an adsorbate-induced missing-row reconstruction of the substrate (shown in Fig. 5) is consistent with both the LEED and HREELS data. In this case, the O atom is really adsorbed in a pseudo-4*F* site with a short Cu–O distance (about 1.9 Å) to the Cu atoms in the top layer and along Cu–O bond to the Ni atoms in the second layer beneath the missing row. Given the possibility that the $(2\sqrt{2}\times\sqrt{2})R\,45°$ and $c(2\times2)$ phases are quite similar, it would be interesting to see if such a feature can be observed with a SEXAFS experiment.

Oxygen-induced substrate reconstructions also appear for the (100) surfaces of Cu and Ni. Baberschke and coworkers[116] initially concluded from SEXAFS data that in the (2×1) phase on the Cu(110) surface O atoms adsorb in long-bridge 2*F*-*L* sites with a bond length of 1.84 Å. Bader *et al.*[58] later modified these conclusions from polarization-dependent data to include a missing-row reconstruction of the type shown in Fig. 6(a), where every other [001] row is missing. In this structure each O atom has two pairs of Cu nearest neighbors situated at about 1.84 and 2.00 Å. This interpretation has been supported by a recent LEED study,[131] but contradicts high-energy ion scattering[132] and scanning tunneling microscopy[133] observations that favor a buckled-row model [Fig. 6(c)]. Both the LEED data of Parkin *et al.*[131] and low-energy ion scattering data[134,135] place the O atoms approximately coplanar with the Cu atoms, and suggest a substantial expansion of the first interlayer spacing d_{12} by 16%. The source of the discrepancies between the various techniques remains to be resolved.

A similar controversy has arisen over the corresponding (2×1) O/Ni(110) phase. Here the SEXAFS studies of Baberschke *et al.*[92,93] support a sawtooth [Fig. 6(b)] rather than a missing-row reconstruction. Here the O atom is postulated to be adsorbed in a 2*F*-*L* site, possibly tilted toward

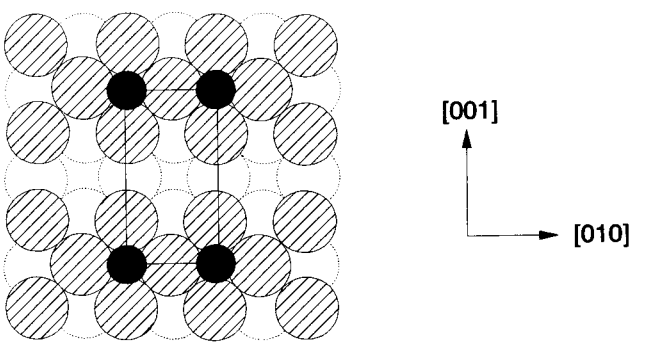

FIG. 5. Missing row reconstruction structure proposed[127,128] for $(2\sqrt{2}\times\sqrt{2})R\,45°$ O/Cu(100).

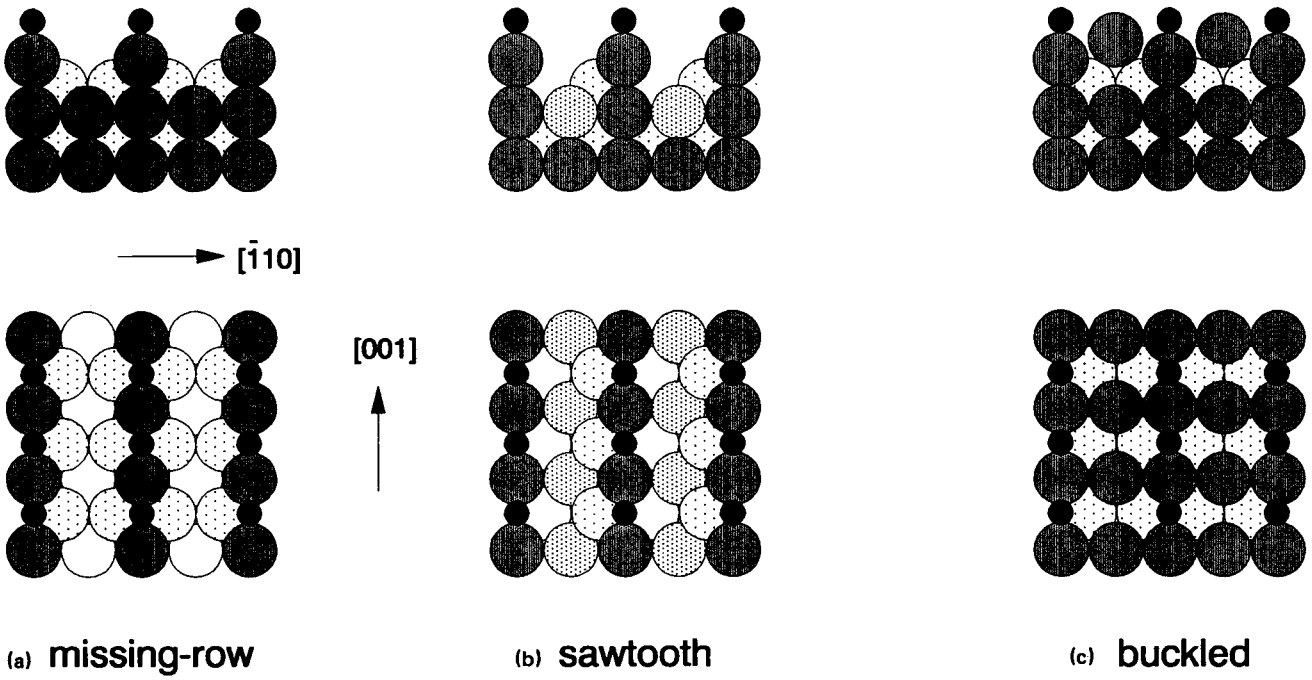

FIG. 6. Possible (2×1) chalcogen-induced reconstructions for an fcc(110) surface. (a) Missing row (MR), (b) sawtooth (ST) and (c) buckled (B).

the (100) facets of the reconstructed substrate. Support for the sawtooth reconstruction has also come from medium energy ion-scattering[144] and scanning tunneling microscopy[145] experiments. On the other hand, other ion-scattering data[146,147] favor the same adsorption site with a missing-row reconstruction. A recent LEED[143] study finds that a missing-row reconstruction is a better fit than either a sawtooth or buckled-row rearrangement. In this study Kleinle *et al.* find a much shorter Ni–O bond length of 1.77 Å, compared with SEXAFS value of 1.85 Å,[92,93] and they also find evidence for vertical relaxations of the Ni interplanar distances—the first being expanded and the second contracted relative to the bulk value. Kleinle *et al.* argue that allowing for an expanded top Ni–Ni interlayer spacing in the SEXAFS analysis, rather than assuming a contraction as did Baberschke *et al.*,[92,93] would remove the preference in the SEXAFS data for a sawtooth over a missing-row reconstruction. Clearly here too there are fundamental discrepancies to be addressed.

Experiments using several different techniques (see Table 4) on the $c(2\times2)$ S/Ni(110) system have, by way of contrast, shown excellent agreement in placing the S atom in the rectangular hollow site on the (110) surface. This site (Fig. 1) has the S atoms bonding to one atom in the second Ni layer at a bond length of 2.23 Å and to four first layer Ni atoms at a distance of 2.31 Å, with the first interlayer Ni spacing being expanded. The case of $p(2\times1)$ oxygen on Ag(110) also appears thus far to involve a straightforward chemisorption system with the O atom adsorbed in the 2*F*-*L* site with SEXAFS,[30] LEED,[157] and low-energy ion scattering[158] experiments in agreement.

Even in the case of the stable (111) surfaces of Cu and Ni there is some evidence that chalcogen adsorption may involve some degree of substrate rearrangement. In the case of the $p(2\times2)$ S/N(111) system the SEXAFS[94] result could not distinguish on which of the two types of 3*F* sites on this surface the S atom was adsorbed, but did produce a bond length of 2.23 Å. This distance is rather longer than those found from LEED[153] (2.10 Å) or ion scattering[154] (2.16 Å). These two studies placed the S atom in the expected fcc 3*F* site with possible small relaxations of the first interlayer spacing of about 3% and lateral shifts of less than 0.03 Å. Initial adsorption of O on Cu(111) is disordered, needing short-range probes for structural elucidation. Here a recent SEXAFS sutdy,[64] supported by low-energy ion-scattering data,[155] suggest that while the O aoms reside in the 3*F* hollow sites, they are very close to coplanar (within $\pm$ 0.2 Å) with the top layer of Cu atoms. The large Cu–Cu distance in the nearest-neighbor shell on the surface is close to that for Cu_2O. This implies that even at coverages near 0.5 ML at room temperature the surface is reconstructing to form an oxide precursor that might be similar to the one obtained after oxygen adsorption at elevated temperatures and subsequent annealing.[156]

A reconstruction of another sort may be occurring in the case of Te on Cu(111). This system has been investigated by Citrin and co-workers by SEXAFS[54] who find an unusual geometry where the Te apparently resides in a sixfold quasi-substitutional site.

Measuring SEXAFS data from low-*Z* adsorbates is generally difficult, but the corresponding SEELFS experiments are more tractable and hence there have been a num-

ber of SEELFS sutdies of C adsorption on metals. Experience has shown that C adsorption via decomposition of a hydrocarbon or CO at low temperatures usually leads to a "carbidic" form of carbon on the surface. Adsorption at high temperatures, or heating a carbidic C overlayer, can proceed in two ways. For the more reactive metals dissolution or bulk carbide formation may occur, or for more noble metals the formation of a graphitic layer is common. Behavior of the first sort has been observed by SEELFS for C on Co[45] and Fe[66] where there is some evidence for the formation of some kind of surface carbide. The authors speculate that surface Co_2C-like[45] or Fe_3C-like[66] layers form, but the data are really insufficient to permit a firm interpretation.

There have been several SEELFS studies of graphitic C layers formed by the high-temperature (300–600 °C) decomposition of CO on Cu(110),[55] Ni(110),[91] and (111)[96] surfaces. In the case of Ni(111) there is a simple match of the graphite lattice to the substrate if the C–C bond distance is lengthened slightly to 1.45 Å from 1.42 Å. The single C–Ni bond length of 3.1 Å from the SEELFS data places the C atoms 2.8 Å above the Ni layer. By monitoring the Ni M_{23} fine-structure Rosei *et al.*[96] were also able to tell that the Ni–Ni distances in the substrate had not changed. For the Cu and Ni(110) surfaces there is no such simple match of the graphite lattice with the substrate, but by stretching the C–C distance to 1.44 Å (Ni), or 1.47 Å (Cu), the C atoms can match the substrate periodicity in the [110] direction. Matching the radial distribution from the Fourier transform of the SEELFS data with model calculations favors a structure with the graphite hexagons centered over the middle of the (110) rectangles with a threefold symmetry axis as shown in Fig. 7. Here the C atoms are of three types, labeled A–C, with different first-shell coordinations; these are shown in Table 5 with the experimental and model C–metal distances. Again monitoring the Ni M_{23} signal revealed no significant changes in metal–metal spacings, perhaps a somewhat surprising result in view of the earlier discussion where substrate rearrangements appear to be a common feature of atomic adsorption. While the agreement between experiment and the model predictions is quite good for Cu(110), the radial distribution function for the Ni system is so broad, much more so than the corresponding Cu data, that all the first-shell coordination distances are contained within it, hence leaving some doubt as to the uniqueness of the model. A striking feature of the Ni and Cu(110) results is that the height of the C atoms above the surface is apparently much less than that in the Ni(111) case.

TABLE 5. Surface bond lengths (d) in Å and coordination numbers (CN) from SEELFS investigations of the first shell for each type of atom shown in Fig. 7 for graphitic carbon on Cu and Ni(110) surfaces.

		Cu(110)[55]		Ni(110)[95]	
Atom type	CN	d(model)	d(exptl).	d(model)	d(exptl.)
A	5	2.55	2.71	2.49	
B	1	1.66		1.95	2.40
			1.78		
C	2	1.83		1.95	

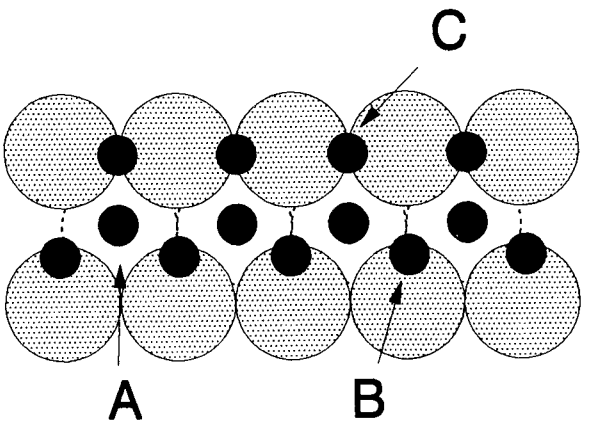

FIG. 7. Proposed structure from SEELFS measurements for graphitic C on the (110) surfaces of Cu[55] and Ni[95]. The C atoms (filled circles) are of three types (A–C) with different coordinations (see Table 5).

Interestingly, carbon on the Ni(100) surface does not appear to undergo a carbidic to graphitic transformation like that seen on the (110) surface. Adsorption of ethylene on Ni(100) and heating to 400–500 K yields a layer of carbidic carbon and an unusual LEED pattern designated $p4g(2\times2)$. This pattern is similar to a normal (2×2) pattern but with systematic absences indicating that a reconstruction has occurred that includes a glide plane of symmetry. This system was first investigated by Onuferko *et al.*[159] by LEED and was found to involve C atoms occupying 4*F* sites that induce a distortion, best described as a rotation, of the top layer of Ni atoms as shown in Fig. 8. This system has since been reinvestigated by both SEELFS[78,79] and SEXAFS[80] with the results shown in Table 6, which agree with the site and sense of reconstruction. The SEELFS study of Chiarello *et al.*[79] did not explicitly confirm that a $p4g(2\times2)$ LEED pattern was present and did use quite different preparation conditions from the other studies. All the fine-structure investigations were hampered by a lack of experiment C–Ni phase shifts and therefore used either experimental O–Ni phase shifts[3] (Atrei *et al.*[78] and Bader *et al.*[80]) or theoretical C–Ni shifts[21] (Atrei *et al.*[78] and Chiarello *et al.*[79]). Unfortunately, as Table 6 underscores, the derived bond lengths are critically dependent upon this choice; in order to obtain agreement with the LEED results the experimental O–Ni phase shifts must be employed.

The first shell C–Ni bond length of about 1.8 Å found for this system imply that the C atoms must lie very close, within 0.2 Å or so, of the top layer of Ni atoms. Both SEXAFS[80] and SEELFS[78] data show a second feature in the Fourier transform that would correspond to a second C–Ni distance of about 3 Å. The origin of this feature is somewhat mysterious. It has approximately the same SEXAFS polarization dependence as the main peak[80] and hence indicates a spacing predominantly parallel to the surface. The model shown in Fig. 8 would predict a second nearest-neighbor distance of about 3.2 Å. Whether this feature is an artifact

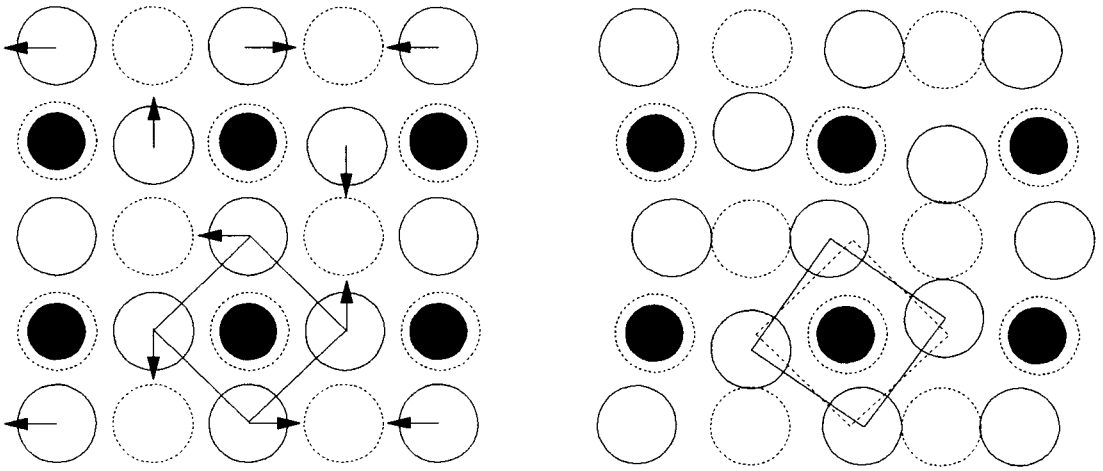

FIG. 8. Model for the $p4g(2\times2)$ Ni(100)–C structure;[78–80,159] filled circles are C atoms (a) unreconstructed $p(2\times2)$ structure with arrows depicting the sense of the distortion in the top Ni layer, (b) reconstructed $p4g(2\times2)$ structure.

due to multiple scattering, or an indication that the model of Fig. 8 should be modified is not yet clear.

It is interesting to note that the $p4g(2\times2)$ structure shown in Fig. 8 has also been shown to fit SEXAFS[85,86] and photoelectron diffraction[160] data for the equivalent N adsorption system. The origin of the difference from the O adsorption system discussed earlier remains to be identified.

Only a few examples of metal-on-metal adsorption systems have been explored with SEXAFS to date—Cs/Ag(111),[27,32] Pb/Ag(111),[34] Cu/Au(111),[36] Ag/Au(111),[40] and Co/Cu(111).[62,63] In the latter investigation, the authors attempted to determine the anisotropy of the surface Debye–Waller factor from relative temperature-dependent amplitude functions for two different polarizations. The elegance of this method is that no backscattering amplitudes of phase shifts are required, and any static disorder is eliminated. In this case, for a (1×1) overlayer of Co on Cu(111), Rougin *et al.*[62] and Chandesris *et al.*[63] found that the mean-square relative displacement of the Co atoms parallel to the surface is close to the bulk value, while in the normal direction it is larger by about 25%. However, this result has been criticized by Citrin.[6]

An exciting new area of SEXAFS investigations is the *in-situ* determination of surface geometries at working electrode surfaces. Melroy, Blum, and co-workers have studied underpotentially deposited lead on silver electrodes[34] and copper[36] and silver[40] on gold electrodes, the electrodes being grown on mica. They used fluorescence detection at grazing incidence excitation in an electrochemical cell but were still hampered by a poor signal-to-noise ratio. The SEXAFS from Pb/Ag(111)[34] contained no detectable contribution from Pb–Ag scattering, either because the lead was adsorbed incommensurately with the Ag substrate, or possibly because of large thermal motions of the lead atoms. The fine structure was attributed to scattering from oxygen atoms belonging to adsorbed water or acetate ions. It is apparent that the RDF from these data contains a large peak at about 1.7 Å; it is possible that this may be an artifact due to a Ramsauer–Townsend resonance[6] and not therefore interpretable in terms of surface structure. The same group had more success with Cu[36] and Ag[40] deposited on Au(111) where both metal–Au and metal–O scattering could be detected resulting in a structure where the adsorbate metal atoms sit above the $3F$ sites on the Au(111) surface with water or a solution anion bonded at a well-defined distance. This same adsorption site has also been identified in a LEED investigation of the Ag/Au system,[161] but in this case the Ag was evaporated in vacuum.

An unusual and controversial example of the use of SEXAFS in metal-on-metal systems are the studies of ther-

TABLE 6. Surface bond lengths for chemisorption of C on Ni(110) in $4F$ sites for the $p4g(2\times2)$ structure (see Fig. 8) from fine structure and other techniques.

Method	Ref.	Phase shifts	$d(\text{C–Ni})_1$ (Å)	$d(\text{C–Ni})_2$ (Å)
SEXAFS	80	O–Ni(ex)[a]	1.82 ± 0.05	2.9 ± 0.1
SEELFS	78	O–Ni(ex)[a]	1.85 ± 0.05	3.1 ± 0.1
		C–Ni(th)[b]	1.78 ± 0.05	3.0 ± 0.1
SEELFS	79	C–Ni(th)[b]	1.75 ± 0.05	2.9 ± 0.1
LEED	159	···	1.80 ± 0.02	···

[a] (ex) indicates experimental phase shifts from Ref. 3.
[b] (th) indicates theoretical phase shifts used from Ref. 21.

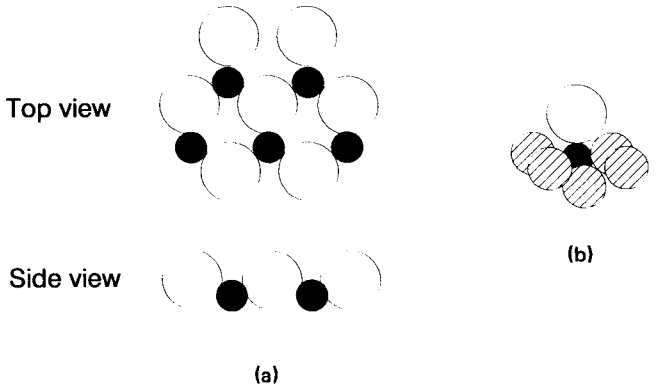

FIG. 9. Models from SEXAFS data for the structure of BaO/W thermionic cathode surfaces with large open circles for Ba, shaded circles for W and small stippled circles for O; (a) a BaO unit adsorbed on W(211) of Norman *et al.*[111,112] and (b) a BaO layer incommensurate with W of Shih *et al.*[113]

mionic BaO/W cathode surfaces by Norman *et al.*[111,112] and Shih *et al.*[113] Here both groups apparently used standard cathodes with very similar work functions and BaO coverages. The SEXAFS data from the Ba $L_{2,3}$ edge from the two studies is quite similar, but the radial distribution functions do show some significant amplitude differences. The two groups come up with rather different structures. Both groups have O as the nearest neighbor to Ba but, whereas Norman *et al.*[111,112] place a single O atom at a distance of 2.62 Å, Shih *et al.*[113] have a shell of 3 O atoms 2.33 Å from the Ba. To further confuse matters, Shih *et al.* find the second nearest-neighbor shell to be 6 Ba atoms at 3.40 Å, while Norman *et al.*[111,112] find 4 W atoms at 3.59 Å. The results of Norman *et al.* favor a model [Fig. 9(a)] in which a single BaO unit is adsorbed in, for example, the hollow site on a W(211) plane. The other set of results favors a BaO layer that is incommensurate with any low index face of W [Fig. 9(b)], with close contact to the W for both the Ba and O atoms. The lack of any identifiable Ba–W scattering in this case is surprising, but Shih *et al.* claim that the backscattering amplitude from the second shell closely resembles that of the Ba neighbor in bulk BaO, and is much closer in appearance to the theoretical Ba backscattering amplitude than to the corresponding W amplitudes. They also claim that in the region of k space of interest, the Ba–W scattering, may be swamped by Ba–Ba scattering.

5.1.b. Molecular Adsorption

Because of the initial difficulties of making SEXAFS measurements for low-Z elements the number of such investigations involving molecular adsorbates is rather few. The best studied system of this class is that of formic acid adsorbed on Cu surfaces, using the O K SEXAFS signal in a partial yield mode, often coupled with NEXAFS and PED information. The results are summarized in Table 7; unfortunately there are no corresponding LEED or ion-scattering results. Outka *et al.* performed the first measurements for

TABLE 7. Structural determinations for formate adsorbed on Cu surfaces from fine structure techniques (after Ref. 163).

Surface	Method	Ref.	Formate site[a]	d(Cu–O) (Å)
Cu(100)	SEXAFS	48, 115	Cross-bridge (a)	2.30 ± 0.05
	SEXAFS (reanalysis)	49, 50	Diagonal atop (b)	1.99 ± 0.10
	PED	163	Aligned bridge (c)	1.98 ± 0.04
Cu(110)	SEXAFS	52, 56	Aligned atop (d)	1.94 ± 0.07
	PED	163	Aligned bridge(e)	1.98 ± 0.04

[a] See Fig. 10.

the Cu(100) surface.[48,115] Using room temperature data taken at two angles they proposed, via a single shell analysis, a bidentate formate structure shown in Fig. 10(a) with two equivalent Cu–O distances of 2.38 ± 0.03 Å and the O atoms in 4F sites on the Cu(100) surface. From both NEXAFS and SEXAFS data the C–O bond length is about 1.27 Å, which necessitates that the O atoms are slightly displaced from the center of the 4F hollow sites. This geometry is in good agreement with high resolution electron energy loss spectroscopy data[162] and with the bidentate bonding geometry observed in copper formate complexes,[115] although the Cu–O bond length is unusually long when compared with bulk systems. Outka *et al.* atttribute this large chemisorption bond length to steric constraints imposed by the rigid geometry of the Cu surface atoms.

Woodruff and co-workers[49,50] reexamined these data using a multishell approach and came to quite different conclusions. They argue that substantial interference between the SEXAFS signals from similar but different Cu–O bond lengths occurs due to the low adsorption site symmetry of the O atoms caused by the mismatch between the O–O and Cu–Cu distances. Hence a single shell approach can yield misleading results. Their multishell analysis indicates that, rather than adopting the structure proposed by Outka *et al.* where the formate as a whole resides in a cross-bridged position with the O atoms close to 4F sites, formate instead bonds atop of a Cu atom diagonally aligned along ⟨100⟩ as shown in Fig. 10(b). This results in a much longer Cu–O bond length of 1.99 ± 0.10 Å that is more in accord with known bond lengths.

Woodruff and co-workers also measured and analyzed data for formate adsorbed on Cu(110).[52,56] Here they found an adsorption site very similar to that they proposed for Cu(100). As Fig. 10(d) shows, the formate sits atop a Cu atom diagonally along ⟨110⟩ with a Cu–O distance of 1.98 Å.

As Table 7 shows, the situation has become clouded recently when these same workers conducted photoelectron diffraction (PED) experiments[163] on these two systems. The modulation structure of the PED signal from the C 1s and O 1s levels of formate are identical on both Cu surfaces, implying that the adsorption site on both is the same. The Cu–O

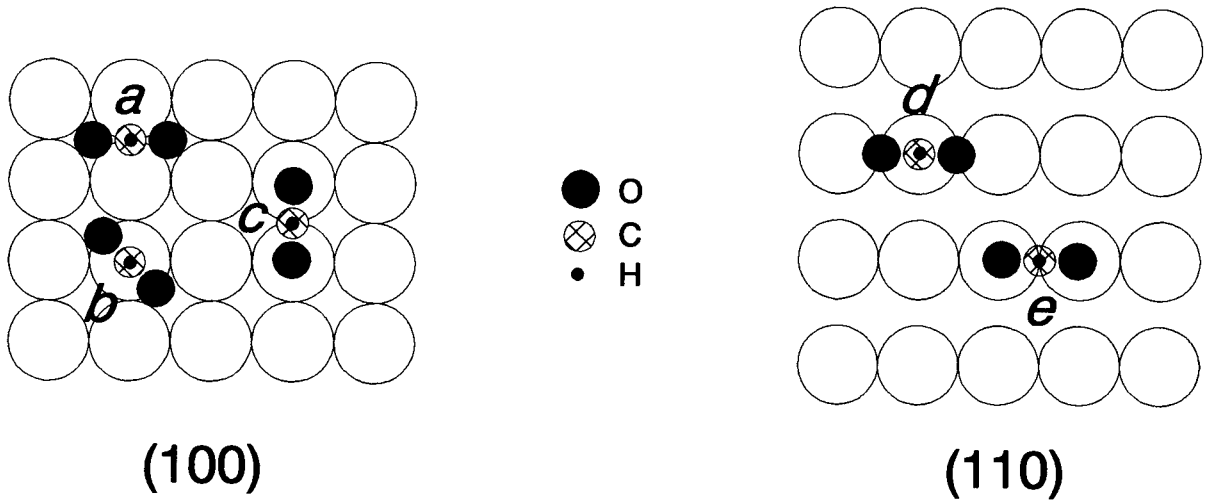

FIG. 10. Proposed SEXAFS-derived structures for formate adsorbate on Cu surfaces. On Cu(100) (a) cross-bridge model of Outka *et al.*[47,115] (b) Diagonal atop model of Crapper *et al.*[49,50] (c) Aligned bridge model of Woodruff *et al.*[163] and on Cu(110) (d) aligned atop model of Crapper *et al.*[52,56] and (e) aligned bridge model of Woodruff *et al.*[163]

bond length they derive of 1.98 Å agrees with their earlier results but the calculations suggest that formate adsorbs in an aligned (short) bridge site on both surfaces, with the O atoms in on-atop sites, as depicted in positions c and e of Fig. 10. They attribute the discrepancy between the SEXAFS and PED results as due to a failure to recognize that the grazing incidence SEXAFS are dominated by Cu backscattering, whereas the normal incidence SEXAFS is dominated by O backscattering. As the determination of the adsorption site via SEXAFS is generally found through the dependence of the amplitudes on the direction of polarization of the x rays, then O–O intramolecular scattering in particular may lead to ambiguities in the derived adsorption site. There are, however, some quantitative difficulties that remain in reconciling these two sets of experiments and the structure must be regarded as in dispute.

Outka *et al.*[48] also investigated methoxy/Cu(100). They could not unequivocally decide on the adsorption site, but the atop site was ruled out. The Cu–O distance in this case was very similar to that for formate/Cu at 1.97 ± 0.05 Å, and the C–O bond axis was determined to be tilted by about 30° with respect to the surface normal.

The surface structures of adsorbed hydrocarbons have been relatively extensively studied by LEED but have been slow to emerge from fine-structure techniques. This is probably due to their fragile nature that would lead to decomposition under a SEELFS electron beam, and to the weak SEXAFS beckscattering from carbon. Nevertheless Baberschke and co-workers have studied the C *K* edge from acetylene and ethylene adsorbed on Cu(100)[47] using the total electron yield and a high beam flux. From a previous NEXAFS investigation,[164] they had concluded that the molecules lie flat on the surface. They used the experiment N–C phase shift from Cu phthalocyanine and neglected the H atoms in the molecules in fitting simulated SEXAFS oscillations for a large number of model compounds. The results, collected in Table 8, are interesting. For ethylene the C atoms are located symmetrically 1.25 Å above the first layer of Cu atoms [Fig. 11(a)]. On the other hand, the best fit for acetylene was the so-called μ_3 site with the C–C axis parallel to the main diagonal of the unit cell and each C atom is equidistant to two Cu nearest neighbors, shown in Fig. 11(b). This type of site for acetylene adsorption has been supported by ultraviolet photoelectron spectroscopy[165] and cluster calculations.[166] The derived C–C bond lengths of 1.42 ± 0.05 Å for C_2H_2 and 1.47 ± 0.07 Å for C_2H_4 are elongated by 0.22 and 0.13 Å, respectively, from the gas phase species, in good agreement with NEXAFS estimates.[164] Even given the large error bars on the SEXAFS results the elongation of the C–C bond on adsorption is apparent.

5.2. Nonmetal Systems

5.2.a. Silicon

Fine-structure studies on semiconductors have concentrated on halogen, chalcogen, and metal adsorbates on silicon, although the III–V semiconductors have recently received more attention. Some of the first experiments were performed by Citrin and co-workers on the adsorption of Cl, I, and Te on (111) surfaces of Si and Ge. The results have

TABLE 8. Structural determination by SEXAFS[47] for unsaturated hydrocarbons adsorbed on Cu(100).

Adsorbate	Site[a]	d(Cu–C)$_1$ (Å)	d(Cu–C)$_2$ (Å)	d(C–C) (Å)
C_2H_4	Symmetric	1.87 ± 0.05	3.16 ± 0.05	1.42 ± 0.05
C_2H_2	μ_3	1.86 ± 0.07	2.70 ± 0.07	1.47 ± 0.07

[a] See Fig. 11.

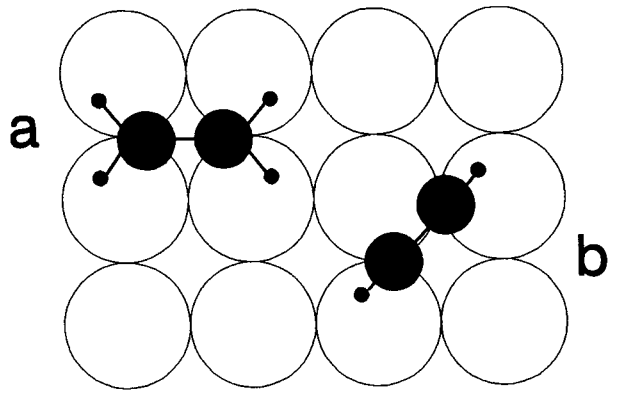

FIG. 11. Adsorption sites proposed from SEXAFS measurements for unsaturated hydrocarbons on Cu(100)[47]; C_2H_4 in symmetric site and (b) C_2H_2 in μ_3 site.

TABLE 9. Adsorption sites and bond length for nonmetal atomic species adsorbed on Si and Ge surface from SEXAFS experiments.

Substrate (S)	Ref.	Adsorbate (X)	Adsorption site[a]	d(X-S) (Å)
Si(111)	69,70 102	Cl	1*F*	2.03 ± 0.03
	104	Ge	3*F*[b]	2.30 ± 0.02
	69,70 71	I	1*F*	2.44 ± 0.03
	69.70 71	Te	2*F*	2.47 ± 0.03
Si(100)	99	O	2*F*	1.65 ± 0.02
Ge(111)	69,70 102	Cl	1*F*	2.07 ± 0.03
	69,70 71	I	1*F*	2.50 ± 0.04
	69,70 71	Te	3*F*′	2.7

[a] See Fig. 12.
[b] See text.

been summarized[69,70] and are collected together in Table 9. The experiments were carried out on the reconstructed clean Si(111) (7×7) and Ge(111) (2×8) surfaces at a time when these reconstructions were not well understood, prior to the key LEED, STM, electron microscopy, and ion-scattering experiments that led to the unravelling of these complex structures.[1,2] However, the authors argued that any long-range reconstruction would be relieved by chemisorption, at least within the range sampled by SEXAFS measurements, and assumed the substrates to be unreconstructed. In contrast to metal surfaces, semiconductor surfaces have strongly directional bonding and hence we might not expect overlayer structures on Si or Ge(111) to necessarily bear any resemblance to those seen on close-packed metal surfaces. Citrin *et al.*[69] proposed that sensible arguments can be made to support adsorption into any of the four most symmetric sites on a Ge or Si(111) (1×1) surface shown in Fig. 12. They indeed found an interesting variety of adsorption site preferences (see Table 9 and Fig. 12). While both Cl and I appear to adsorb in an atop 1*F* site on both surfaces, Te apparently adsorbs in a 2*F* bridge site on Si(111) but in a 3*F* site, with a substrate atom under, on Ge(111).

There have been several investigations aimed at understanding the process of Si oxidation.[99,100,107] These studies have been hampered by difficulties concerning changes in structure as a function of O uptake due to penetration into the substrate. Perhaps the clearest results are those of Incoccia *et al.*[99] who studied a 1ML coverage of O on Si(100), the point where the clean surface (2×1) reconstruction is lost. They found O atoms occupying two types of bridge positions: one a normal chemisorption site and a second between the two topmost layers of Si atoms.

Comin *et al.*[104] studied the Si(111)7×7:Ge interface prepared at room temperature. At about 1.5 ML coverage they find a coordination around the Ge absorbers of 2.6 ± 0.3 Ge atoms at 2.44 ± 0.02 Å, and 1.4 ± 0.3 Si atoms at 2.30 ± 0.02 Å. The Ge–Ge bonds are about the same length as in the bulk, but the Ge–Si bonds are compressed relative to the value of 2.38 Å found in amorphous alloys. The authors base their structural model on the generally accepted dimer–adatom stacking fault (DAS) description[167] of the Si(111) (7×7) reconstruction shown in Fig. 13(a). RHEED data[168] show that the reconstruction still persists under the Ge overlayer at this coverage. They argue that their data are consistent with Ge atoms bonding together to form chains running parallel to the surface while adjacent chains are bridged by other Si chains as shown in Figs. 13(b) and 13(c). This structure is also consistent with ion scattering data,[169,170] whereas a simple bulk-like double layer of Ge and Si atoms, a possible structure consistent with the SEXAFS data, is not. There are two further points of interest. The structure shown in Figs. 13(b) and 13(c) must

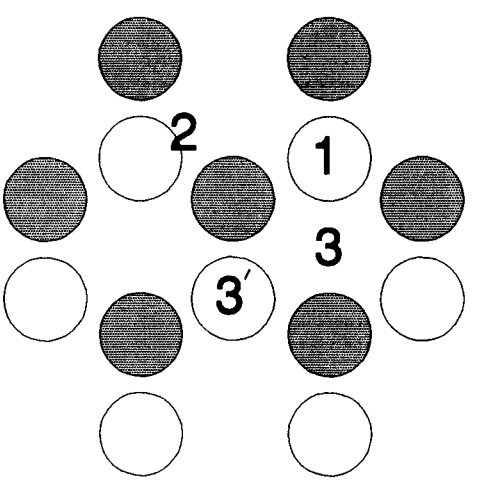

FIG. 12. High symmetry adsorption sites on unreconstructed Si or Ge(111) surfaces. Top layer substrate atoms are shown shaded and second layer atoms open.

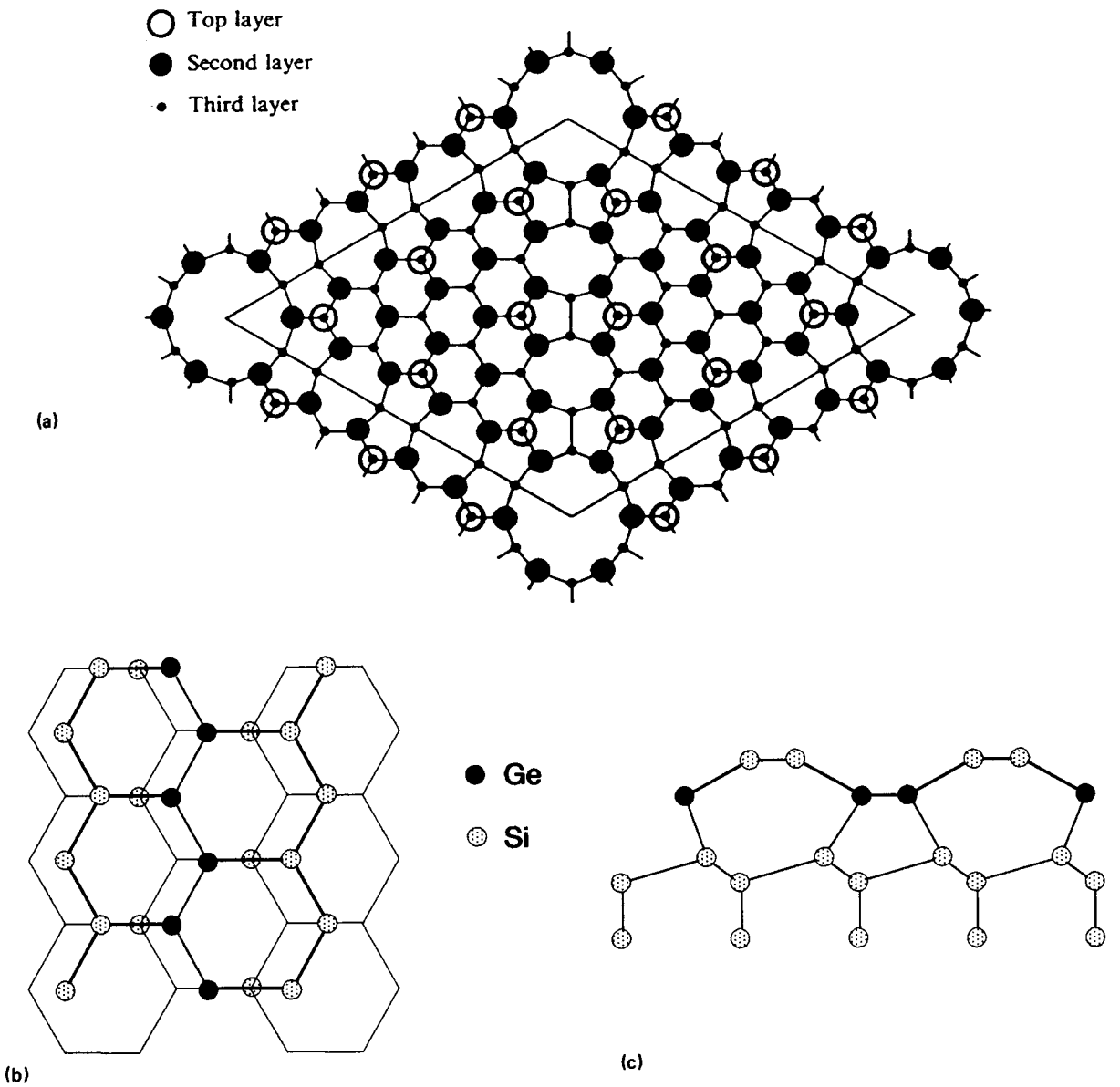

FIG. 13. (1) dimer–adatom stacking fault (DAS) structure[169] for the Si(111) (7×7) reconstruction, (b) top view SEXAFS model[104] for 1 ML Ge on Si(111), (c) side view of (b).

terminate or cross over the boundaries of the triangular subunits of (7×7) cell to preserve the reconstruction under the Ge layer. Also the Si adatoms of the DAS structure must displace to allow for the formation of the Ge chains, but far more Si atoms are needed to form complete Si chains. Possibly the additional Si is provided by step consumption. As the Ge coverage is increased there is an increasing buildup of strain in the system so that at 3 ML coverage an amorphous Ge layer with embedded Si is present.

There have been a number of SEXAFS studies of metal overlayer–Si systems directed at understanding Schottky barrier heights produced by the metal–semiconductor interface. It is probable that the important effects that determine the barrier height occur during the initial stages of metal deposition, perhaps during adsorption of the first monolayer. There appears to be a general trend emerging from SEXAFS, LEED, and ion-scattering studies in this area. At room temperature, noble metals show little tendency for compound formation and show epitaxial, or at least island growth, with perhaps some mixing after annealing. In contrast, more reactive metals such as Co, Ti, Ni, or Pd exhibit silicide formation from the outset of deposition.

Perhaps one of the best studied systems of the first type is Ag/Si(111); it has been the subject of numerous investigations by LEED, RHEED, STM, and various forms of ion scattering. A recent paper by Watamori *et al.*[171] is a good source of references. Perhaps surprisingly, the most recent SEXAFS investigation is that of Stohr *et al.*[101] in 1983. They used polarization data to follow the deposition of Ag on Si(111) (7×7) at coverages up to 3 ML. Room temperature deposition leads to a fading of the (7×7) LEED pattern. As a result Stohr *et al.* assumed that the Si surface relaxes from its reconstructed state at least locally, a finding supported by very recent ion scattering results.[171] At 1/3 ML coverage they determined that the metal chemisorbs in the threefold hollow site, see Fig. 12, approximately 0.7 Å above the outer-

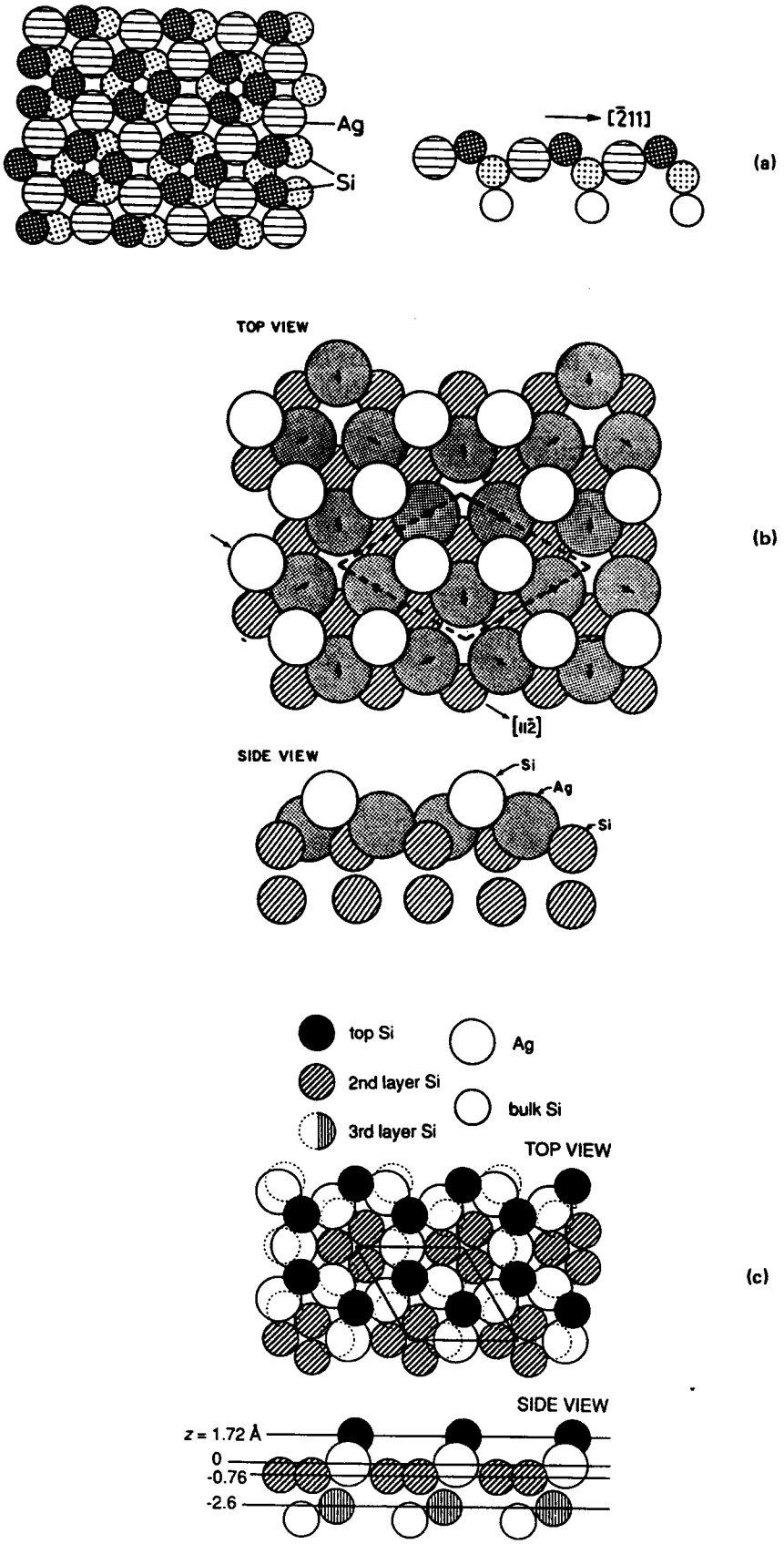

FIG. 14. Various structural models proposed for Ag/Si(111) $(\sqrt{3}\times\sqrt{3})R30$; (a) the honeycomb structure;[173] (b) the trimer model;[176] (c) the silver honeycomb-chained trimer model.[179] [Reprinted with permission of North-Holland from Surf. Sci. **112**, 321 (1981), Fig. 20a; American Institute of Physics from Phys. Rev. Lett. **58**, 1555 (1987), Fig. 4; North-Holland from Surf. Sci. **209**, 111 (1987), Fig. 4.]

most Si atoms, with an average Ag–Si distance of 2.48 ± 0.05 Å. Above a monolayer coverage, the SEXAFS data are consistent with the formation of Ag(111) islands on the surface, as previously suggested by Auger studies.[172]

Annealing a Si(111) surface covered with about 2/3 ML of Ag at 200–600 °C results in a $(\sqrt{3}\times\sqrt{3})R$ °30 (R3) LEED pattern that has been the focus of the bulk of the investigations of this system. The SEXAFS results of Stohr *et al.*[101] place the Ag atoms embedded in the threefold hollow between the first two Si layers, i.e., sixfold coordination, with an Ag–Si distance of 2.48 ± 0.04 Å and is consistent with the honeycomb model [Fig. 14(a)] suggested by Saitoh *et al.*[173] from low-energy ion-scattering data. This model has been recently supported by STM work[174,175] but other STM[176] and RHEED[177] studies favor a trimer model shown in Fig. 14(b). To complicate matters further, the most recent ion scattering work[171,178] indicates that the true structure might involve both of these sorts of structural entity—the silver honeycomb-chained dimer model[179] shown in Fig. 14(c).

The other fine-structure investigations involving metals on Si(111) indicate that silicide formation occurs. The initial stages of reaction appear in all cases to resemble that seen for Ag, that is, the metal atoms penetrate into the sixfold coordinate interlayer site shown in Fig. 15. SEXAFS studies on Ni,[106] Pd,[101b], Pt,[108] and Co[103] all indicate that silicide growth seem to proceed via this site. However, the further growth of the silicide layer from this point can vary from metal to metal. Thus $CoSi_2$ and $NiSi_2$ are two chemically similar silicides that can be grown epitaxially on Si(111). The SEXAFS studies on Ni of Comin *et al.*,[106] supported by ion scattering data,[180] reveal that Ni atoms initially penetrate into the sixfold hollow between the first and second Si layers, weakening Si–Si bonds. The Si atoms expand to form a $NiSi_2$-like structure and further Ni adsorption and diffusion leads to a $NiSi_2$–Si(111) interface, as shown in Fig. 16(a), where the Ni atoms are 7-coordinate rather than 8-coordinate as in the bulk material. However, the work of Rossi *et al.*[103] on the $CoSi_2$–Si(111) interface indicates that here the Co atoms are indeed 8-coordinate as in bulk $CoSi_2$ [see Fig. 16(b)].

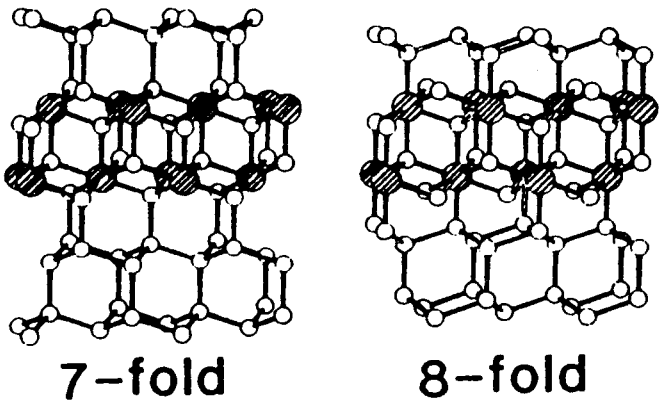

FIG. 16. Models for MSi_2–Si(111) interfaces, where M = transition metal, involving; (a) sevenfold and (b) eightfold coordinate metal atoms. Metal atoms are shown shaded. [Reprinted with permission of the American Institute of Physics from Phys. Rev. Lett. **62**, 191 (1989), Fig. 1.]

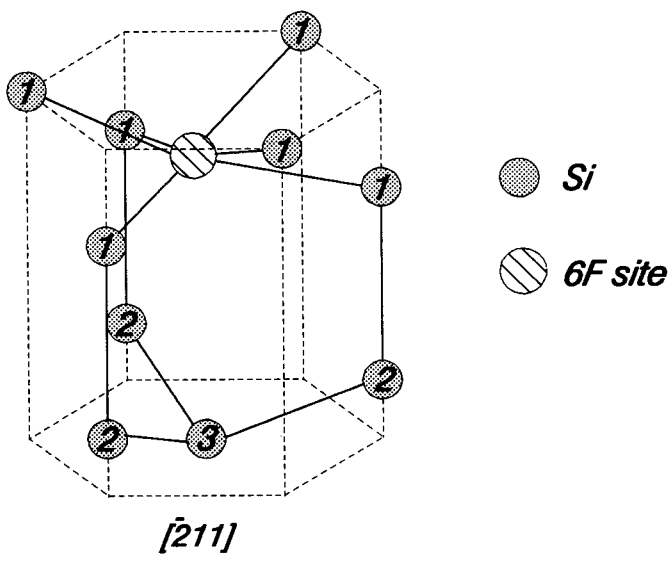

FIG. 15. The six-coordinate interlayer adsorption site adopted in many metal–Si(111) systems. Adapted from Ref. 108.

5.2.b. Other Semiconductors

SEXAFS or SEELFS studies on semiconductors other than Si or Ge are very few in number. An early study of oxygen adsorption on GaAs(110) by Stohr *et al.*[68] was inconclusive and clearly could benefit from repetition under more modern conditions that would allow a better signal-to-noise ratio. Choudary and co-workers[39] have developed a new variant of the SEXAFS technique employing photoemission to detect the fine structure with high sensitivity. They have used this PEXAFS method to study the (110) surface of InP both clean[72,73] and covered with very small amounts of Al[72] and Na.[74] The clean InP(110) surface is known from extensive LEED studies[181] to show a subtle reconstruction depicted in Fig. 17. Here the surface is relaxed from its bulk configuration by bond rotations in the first bilayer of about 27° which induce vertical (anion out and cation in) and horizontal movements of the surface atoms, resulting in a small contraction of the first bilayer toward the bulk. The PEXAFS results on the clean surface[72,73] show a 4% contraction of the P–In bond length that is in good agreement with the LEED study of Duke and co-workers.[181] The PEXAFS results also indicated that the surface unit mesh parameter a_0 is also contracted by 0.09 ± 0.05 Å, an effect not noted in the LEED work. When even very small amounts of Al[72] or Na[74] are adsorbed on a clean InP(110) surface, the PEXAFS data indicate that the surface unit mesh relaxation is removed and drastic reconstruction involving the in-plane In–P bonds change occurs, although the

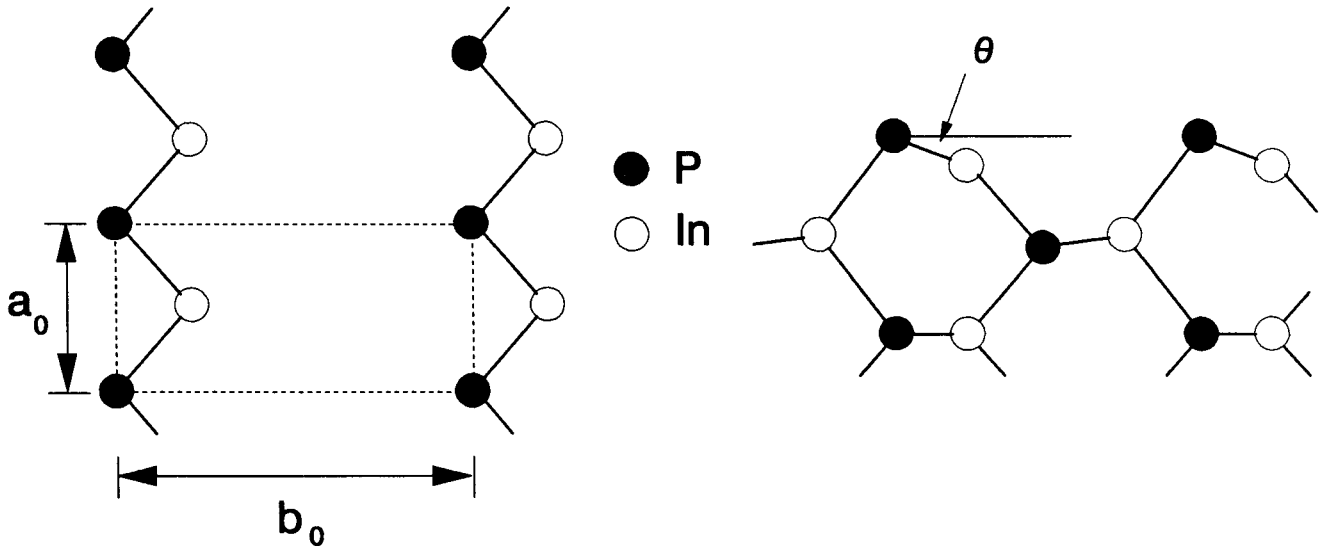

FIG. 17. Schematic of the atomic geometry of the reconstructed InP(110) surface showing the bond rotation (θ); (a) top view, (b) side view. Adapted from Ref. 181.

exact location of the In atoms has not been determined.

The II–VI semiconductors are yet to be examined to any real extent by fine-structure methods. The lone example to date is a SEELFS study of polycrystalline ZnO[114] that resulted in a nearest-neighbor spacing of the surface atoms that was slightly longer (by 0.07 Å) than that in the bulk.

5.2.c. Other Nonmetals

Fine-structure experiments on nonmetals other than common semiconductors are quite rare. A brief SEELFS study on polycrystalline boron[41] appeared to show a considerable reduction in the B–B surface bond lengths, but this work is compromised by the indeterminate nature of the surface after sputtering. We include here for completeness some early SEXAFS studies on high surface area carbon (Grafoil) carried out in the straight absorption mode by Stern and co-workers who studied the physisorption of Br[43] and Kr.[44] Bromine molecules adsorb at room temperature with one atom fixed above the hexagonal site of the graphite basal plane while the other atom is free to move. Natarajan and coworkers[42] have employed SEELFS to measure the first-shell coordination numbers and bond lengths in diamond, pyrolytic graphite, and "Aquadag"—an aqueous suspension of graphite particles.

6. Acknowledgments

The author gratefully acknowledges the help of Ms. Sheila Lidwill and Dr. Scott Mokler in locating many of the papers.

This work was supported by the National Institute of Standards and Technology Critical Compilation of Physical and Chemical Reference Data Program through Grant No. 60NANB9D0987.

7. References

[1]P. R. Watson, J. Phys. Chem. Ref. Data **16**, 953 (1987).
[2]P. R. Watson, J. Phys. Chem. Ref. Data **19**, 85 (1990).
[3]J. Stohr, in *X-ray Absorption, Principles, Techniques, Applications of EXAFS, SEXAFS and XANES*, edited by R. Prins and D. C. Koningsburger (Wiley, New York, 1988), Chap. 10.
[4]D. P. Woodruff, Surf. Interface Anal. **11**, 25 (1988).
[5]P. H. Citrin, Surf. Sci. **184**, 109 (1987).
[6]P. H. Citrin, J. Phys. C **8**, 437 (1986).
[7]D. Norman, J. Phys. C **19**, 3237 (1986).
[8]J. Stohr, Z. Phys. B **61**, 439 (1985).
[9]J. Haase, Appl. Phys. A **38**, 181 (1985).
[10]J. Stohr, R. Jaeger, and S. Brennan, Surf. Sci. **117**, 503 (1982).
[11]P. Eisenberger, P. Citrin, R. Hewitt, and B. Kincaid, CRC Crit. Rev. Solid State Mater. Sci. **10**, 191 (1981).
[12]M. De Crescenzi, CRC Crit. Rev. Solid State Mater. Sci. **15**, 279 (1989).
[13]M. De Crescenzi, Surf. Sci. **162**, 838 (1985).
[14]J. Stohr and D. A. Outka, J. Vac. Sci. Technol. A **5**, 919 (1987).
[15]B. K. Teo, *EXAFS: Basic Principles and Data Analysis* (Springer-Verlag, Berlin, 1986).
[16]R. Jaeger, J. Feldhaus, J. Stohr, Z. Hussain, D. Menzel, and D. Norman, Phys. Rev. Lett. **45**, 1870 (1980).
[17]E. A. Stern, Phys. Rev. B **10**, 3027 (1974).
[18]G. Lamble and D. A. King, Philos. Trans. R. Soc. London Ser. A **318**, 203 (1986).
[19]P. Eisenberger and G. S. Brown, Solid State Commun. **29**, 481 (1979).
[20]P. H. Citrin, P. Eisenberger, and B. M. Kincaid, Phys. Rev. Lett. **36**, 1346 (1976).
[21]B. K. Teo and P. A. Lee, J. Am. Chem. Soc. **101**, 2815 (1979).
[22]B. K. Teo, P. A. Lee, A. L. Simons, P. Eisenberger, and B. M. Kincaid, J. Am. Chem. Soc. **99**, 3854 (1977).
[23]A. G. McKale, G. S. Knapp, and S-K. Chan, Phys. Rev. B **33**, 841 (1986).
[24]P. A. Lee and G. Beni, Phys. Rev. B **15**, 2862 (1977).
[25]E. A. Stern, B. A. Bunker, and S. M. Heald, Phys. Rev. B **21**, 5521 (1980).
[26]D. Briggs and M. Seah, *Practical Surface Analysis by Auger and X-ray Photoelectron Spectroscopy* (Wiley, Chichester, 1983).
[27]G. M. Lamble, D. J. Holmes, D. A. King, and D. Norman, J. Phys. Colloq. C **8**, 509 (1986).
[28]G. M. Lamble, R. S. Brooks, J. C. Campuzano, D. A. King, and D.

Norman, Phys. Rev. B **36**, 1796 (1987).
[29]D. J. Holmes, N. Panagiotides, R. Dus, D. Norman, G. M. Lamble, C. J. Barnes, F. Della Valle, and D. A. King, J. Vac. Sci. Technol. A **5**, 703 (1987).
[30]A. Puschmann and J. Haase, Surf. Sci. **144**, 559 (1984).
[31]G. M. Lamble, R. S. Brooks, S. Ferrer, and D. A. King, Phys. Rev. B **34**, 2975 (1986).
[32]G. M. Lamble, R. S. Brooks, D. A. King, and D. Norman, Phys. Rev. Lett. **61**, 1112 (1988).
[33]P. H. Citrin, P. Eisenberger, and R. C. Hewitt, Phys. Rev. Lett. **41**, 309 (1978).
[34]M. G. Samant, G. L. Borges, J. G. Gordon, O. R. Melroy, and L. Blum, J. Am. Chem. Soc. **109**, 5970 (1987).
[35]A. Bianconi and R. Z. Bachrach, Phys. Rev. Lett. **42**, 104 (1979).
[36]L. Blum, H. D. Abruna, J. White, J. G. Gordon, G. Borges, M. Samant, and O. R. Melroy, J. Phys. Chem. **85**, 6732 (1986).
[37]D. Norman, S. Brennan, F. Leager, and J. Stohr, Surf. Sci. **105**, L297 (1981).
[38]J. Stoehr, L. I. Johansson, S. Brennan, M. Hecht, and J. N. Miller, Phys. Rev. B **22**, 4052 (1980); Phys. Rev. Lett. **43**, 1882 (1979).
[39]S. T. Kim, K. M. Choudary, S. N. Shah, J. H. Lee, G. M. Rothberg, M. L. den Boer, and G. P. Williams, J. Vac. Sci. Technol. A **5**, 623 (1987).
[40]J. H. White, M. J. Albarelli, H. D. Abruna, L. Blum, O. R. Melroy, M. G. Samant, G. L. Borges, and J. G. Gordon, J. Phys. Chem. **92**, 4432 (1988).
[41]L. Fei, Y. Zheng, Q. J. Zhang, and Z. Y. Hua, J. Vac. Sci. Technol. A **5**, 879 (1987).
[42]C. Natarajan, P. B. Abel, and R. W. Hoffman, Appl. Surf. Sci. **21**, 1 (1985).
[43]E. A. Stern, D. E. Sayers, J. G. Dash, H. Schecter, and B. Bunker, Phys. Rev. Lett. **38**, 767 (1977).
[44]C. Bouldin and E. A. Stern, Phys. Rev. **25**, 3462 (1982).
[45]A. Atrei, U. Bardi, G. Rovida, M. Torrini, E. Zanazzi, and M. Maglietta, J. Vac. Sci. Technol. A **5**, 1006 (1987).
[46]P. H. Citrin, D. R. Hamann, L. F. Matheiss, and J. E. Rowe, Phys. Rev. Lett. **49**, 1712 (1982).
[47]D. Arvanitis, L. Wenzel, and K. Baberschke, Phys. Rev. Lett. **59**, 2435 (1987).
[48]D. A. Outka, R. J. Madix, and J. Stoehr, Surf. Sci. **164**, 235 (1985).
[49]M. D. Crapper, C. E. Riley, and D. P. Woodruff, Surf. Sci. **184**, 121 (1987).
[50]M. D. Crapper, C. E. Riley, and D. P. Woodruff, J. Phys. Colloq. C **8**, 487 (1986).
[51]P. H. Citrin, P. Eisenberger, and R. C. Hewitt, Surf. Sci. **89**, 28 (1979).
[52]M. D. Crapper, C. E. Riley, D. P. Woodruff, A. Puschmann, and J. Haase, Surf. Sci. **171**, 1 (1986).
[53]U. Doebler, K. Baberschke, J. Stohr, and D. A. Outka, Phys. Rev. B **31**, 2532 (1985).
[54]F. Comin, P. H. Citrin, P. Eisenberger and J. E. Rowe, Phys. Rev. B **26**, 7060 (1982).
[55]A. Santoni and J. Urban, Solid State Commun. **63**, 257 (1987).
[56]A. Puschmann, J. Haase, M. D. Crapper, C. E. Riley, and D. P. Woodruff, Phys. Rev. Lett. **54**, 2250 (1985).
[57]M. D. Crapper, C. E. Riley, P. J. J. Sweeney, C. F. McConville, D. P. Woodruff, and R. G. Jones, Surf. Sci. **182**, 213 (1987).
[58]M. Bader, A. Puschmann, C. Ocal, and J. Haase, Phys. Rev. Lett. **57**, 3273 (1986).
[59]P. H. Citrin, P. Eisenberger, and R. C. Hewitt, Phys. Rev. Lett. **45**, 1948 (1980); **47**, 1567 (1981).
[60]M. D. Crapper, C. E. Riley, P. J. J. Sweeney, C. F. McConville, D. P. Woodruff, and R. G. Jones, J. Phys. Colloq. C **8**, 533 (1986).
[61]M. D. Crapper, C. E. Riley, P. J. J. Sweeney, C. F. McConville, D. P. Woodruff, and R. G. Jones, Europhys. Lett. **2**, 857 (1986).
[62]P. Roubin, D. Chandesris, G. Rossi, J. Lecante, M. C. Desjonqueres, and G. Treglia, Phys. Rev. Lett. **56**, 1272 (1986).
[63]D. Chandesris, P. Roubin, G. Rossi, and J. Lecante, Surf. Sci. **169**, 57 (1986).
[64]J. Haase and H. J. Kuhr. Surf. Sci. **203**, L695 (1988).
[65]L. Papagno, L. S. Caputi, G. Chiarello, and P. Delogu, Surf. Sci. **175**, L767 (1986).
[66]S. Polizzi, F. Antonangeli, G. Chiarello, and M. De Crescenzi, Surf. Sci. **136**, 555 (1984).
[67]I. Davoli, L. Palladino, S. Stizza, and A. Bianconi, Solid State Commun. **44**, 1585 (1982).
[68]J. Stoehr, R. S. Bauer, J. C. McMenamin, L. I. Johansson, and S. Brennan, J. Vac. Sci. Technol. **16**, 1195 (1979).
[69]P. H. Citrin and J. E. Rowe, Surf. Sci. **132**, 205 (1983).
[70]P. H. Citrin, J. E. Rowe, P. Eisenberger, and F. Comin, Physica B + C **117-118**, 786 (1983).
[71]P. H. Citrin, P. Eisenberger, and J. E. Rowe, Phys. Rev. Lett. **48**, 802 (1982).
[72]K. M. Choudhary, P. S. Mangat, A. E. Miller, D. Kilday, A. Filipponi, and G. Margaritondo, Phys. Rev. B **38**, 1566 (1988).
[73]K. M. Choudhary, P. S. Mangat, D. Kilday, G. Margaritondo, P. Soukiassian, H. I. Starnberg, and Z. Hurych, J. Vac. Sci. Technol. A **6**, 2024 (1989).
[74]K. M. Choudhary, P. S. Mangat, H. I. Starnberg, Z. Hurych, D. Kilday, and P. Soukiassian, Phys. Rev. B **39**, 759 (1989).
[75]A. Santoni, D. B. Tran Thoai, and J. Urban, Solid State Commun. **68**, 1039 (1988).
[76]R. Jaeger, J. Feldhaus, J. Haase, J. Stoehr, Z. Hussain, D. Menzel, and D. Norman, Phys. Rev. Lett. **45**, 1870 (1980).
[77]B. Lairson, T. N. Rhodin, and W. Ho, Solid State Commun. **55**, 925 (1985).
[78]A. Atrei, U. Bardi, M. Maglietta, G. Rovida, M. Torrini, and E. Zanazzi, Surf. Sci. **211-212**, 93 (1989).
[79]G. Chiarello, J. Andzelm, R. Fournier, N. Russo, and D. R. Salahub, Surf. Sci. **202**, L621 (1988).
[80]M. Bader, C. Ocal, B. Hillert, J. Haase, and A. M. Bradshaw, Phys. Rev. B **35**, 5900 (1987).
[81]J. Stohr, E. B. Kollin, D. A. Fischer, J. B. Hastings, F. Zaera, and F. Sette, Phys. Rev. Lett. **55**, 1468 (1985).
[82]R. G. Jones, S. Ainsworth, M. D. Crapper, C. Somerton, D. P. Woodruff, R. S. Brooks, J. C. Campuzano, D. A. King, G. M. Lamble, and M. Prutton, Surf. Sci. **153/153**, 443 (1985).
[83]R. G. Jones, S. Ainsworth, M. D. Crapper, C. Somerton, and D. P. Woodruff, Surf. Sci. **179**, 442 (1987).
[84]R. G. Jones, S. Ainsworth, M. D. Crapper, C. Somerton, and D. P. Woodruff, Surf. Sci. **179**, 425 (1987).
[85]L. Wenzel, D. Arvanitis, W. Daum, H. H. Rotermund, J. Stohr, K. Baberschke, and H. Ibach, Phys. Rev. B **36**, 7689 (1987).
[86]D. Arvanitis, K. Baberschke, and L. Wenzel, Phys. Rev. B **37**, 7143 (1988).
[87]J. Stoehr, R. Jaeger, and T. Kendelewicz, Phys. Rev. Lett. **49**, 142 (1982).
[88]M. De Crescenzi, F. Antonangeli, C. Bellini, and R. Rosei, Phys. Rev. Lett. **50**, 1949 (1983).
[89]R. McGrath, A. A. MacDowell, T. Hashizume, F. Sette, and P. H. Citrin, Phys. Rev. B **40**, 9457 (1989).
[90]S. Brennan, J. Stohr, and R. Jaeger, Phys. Rev. B **24**, 4871 (1981).
[91]L. Papagno and L. S. Caputi, Phys. Rev. B **29**, 1483 (1984).
[92]K. Baberschke, U. Doebler, L. Wenzel, D. Arvanitis, A. Baratoff, and K. H. Rieder, Phys. Rev. B **33**, 5910 (1986).
[93]U. Doebler, L. Wenzel, D. Arvanitis, and K. Baberschke, J. Phys. Colloq. C **8**, 473 (1986).
[94]D. R. Warburton, P. L. Wincott, G. Thornton, D. Norman, C. H. Richardson, F. M. Quinn, and R. McGrath, Vacuum **38**, 241 (1988).
[95]D. R. Warburton, G. Thornton, D. Norman, C. H. Richardson, R. McGrath, and F. Sette, Surf. Sci. **189-190**, 495 (1987).
[96]R. Rosei, M. De Crescenzi, F. Sette, C. Quaresima, A. Savoia, and P. Perfetti, Phys. Rev. B **28**, 1161 (1983).
[97]R. McGrath, I. T. McGovern, D. R. Warburton, G. Thornton, and D. Norman, Surf. Sci. **178**, 101 (1986).
[98]T. Kendelewicz, P. Soukiassian, R. S. List, J. C. Woicik, P. Pianetta, I. Lindau, and W. E. Spicer, Phys. Rev. B **37**, 7115 (1988).
[99]L. Incoccia, A. Balerna, S. Cramm, C. Kunz, F. Senf, and I. Storjohann, Surf. Sci. **189/190**, 453 (1987).
[100]W. Braun, M. Bader, E. Holub-Krappe, J. Haase, and P. Eichinger, Surf. Interface Anal. **10**, 250 (1987).
[101](a) J. Stohr, R. Jaeger, G. Rossi, T. Kendelewicz, and I. Lindau, Surf. Sci. **134**, 813 (1983); (b) J. Stohr and R. Jaeger, J. Vac. Sci. Technol. **21**, 619 (1982).
[102]P. H. Citrin, J. E. Rowe, and P. Eisenberger, Phys. Rev. B **28**, 2299 (1983).
[103]G. Rossi, X. Jin, A. Santaniello, P. DePadova, and D. Chandesris, Phys. Rev. Lett. **62**, 191 (1989).
[104]F. Comin, S. Paolone, and G. Rossi, Surf. Sci. **211-212**, 511 (1989).
[105]H-C. Wang, R-F. Lin, and X. Wang, Surf. Sci. **188**, 199 (1987).
[106]F. Comin, J. E. Rowe, and P. H. Citrin, Phys. Rev. Lett. **51**, 2402 (1983).
[107]J. Stohr, L. Johansson, I. Lindau, and P. Pianetta, Phys. Rev. B **20**, 664

(1979).
[108]G. Rossi, D. Chandesris, P. Roubin, and J. Lecante, Phys. Rev. B **34**, 7455 (1986).
[109]G. Rossi, D. Chandesris, P. Roubin, and J. Lecante, J. Phys. Colloq. C **8**, 521 (1986).
[110]Y. U. Idzerda, E. D. Williams, T. L. Einstein, and R. L. Park, J. Vac. Sci. Technol. A **5**, 847 (1987).
[111]D. Norman, R. A. Tuck, H. B. Skinner, P. J. Wadsworth, T. M. Gardiner, I. W. Owen, C. H. Richardson, and G. Thornton, J. Phys. Colloq. C **8**, 529 (1986).
[112]D. Norman, R. A. Tuck, H. B. Skinner, P. J. Wadsworth, T. M. Gardiner, I. W. Owen, C. H. Richardson, and G. Thornton, Phys. Rev. Lett. **58**, 519 (1987).
[113]A. Shih, C. Hor, D. Mueller, C. R. K. Marrian, W. T. Elam, P. Wolf, J. P. Kirkland, and R. A. Neiser, J. Vac. Sci. Technol. A **6**, 1058 (1988).
[114]R. Konishi, M. Arioka, Y. Kobayashi, and H. Sasakura, Jpn. J. Appl. Phys. Part 1 **27**, 1347 (1988).
[115]J. Stohr, D. A. Outka, R. J. Madix, and U. Dobler, Phys. Rev. Lett. **54**, 1256 (1985).
[116]U. Dobler, K. Baberschke, J. Haase, and A. Puschmann, Surf. Sci. **152/153**, 569 (1985); Phys. Rev. Lett. **52**, 1437 (1984).
[117]M. A. Van Hove and S. Y. Tong, Surf. Sci. **54**, 91 (1976).
[118]Groupe D'Etude des Surfaces, Surf. Sci. **62**, 567 (1977).
[119]E. Zanazzi, F. Jona, D. W. Jepsen, and P. M. Marcus, Phys. Rev. B **14**, 432 (1976).
[120]F. Jona and P. M. Marcus, Phys. Rev. Lett. **50**, 1823 (1983).
[121]P. H. Citrin, D. R. Hamann, L. F. Mattheis, and J. E. Rowe, Phys. Rev. Lett. **49**, 1712 (1982).
[122]M. Maglietta, E. Zanazzi, U. Bardi, D. Sondericker, F. Jona, and P. M. Marcus, Surf. Sci. **123**, 141 (1982).
[123]F. Jona, D. Westphal, A. Goldmann, and P. M. Marcus, J. Phys. C **16**, 3001 (1983).
[124]J. B. Pendry and D. K. Saldin, Surf. Sci. **145**, 33 (1984).
[125]G. Rovida and F. Pratesi, Surf. Sci. **51**, 270 (1975).
[126]M. Bowker and K. C. Waugh, Surf. Sci. **155**, 1 (1985).
[127]H. C. Zeng, R. A. McFarlane, and K. A. R. Mitchell, Surf. Sci. **208**, L7 (1989).
[128]M. Wutting, R. Franchy, and H. Ibach, Surf. Sci. **224**, L979 (1989).
[129]D. J. Godfrey and D. P. Woodruff, Surf. Sci. **105**, 438 (1981).
[130]T. M. Huphens, Nucl. Instrum. Methods B **9**, 277 (1985).
[131]S. R. Parkin, H. C. Zeng, M. Y. Zhou, and K. A. R. Mitchell, Phys. Rev. B **41**, 5432 (1990).
[132]R. Fiedenhans'l and I. Stensgaard, Surf. Sci. **133**, 453 (1983).
[133]F. M. Chua, Y. Kuk, and P. J. Silverman, Phys. Rev. Lett. **63**, 386 (1989).
[134]E. Van der Riet, J. B. J. Smeets, J. M. Fluit, and A. Niehaus, Surf. Sci. **214**, 111 (1989).
[135]J. A. Yarmoff, D. M. Cyr, J. H. Huang, S. Kim, and R. S. Williams, Phys. Rev. B **33**, 3856 (1986).
[136]P. M. Marcus, J. E. Demuth, and D. W. Jepsen, Surf. Sci. **53**, 501 (1975).
[137]M. A. Van Hove and S. Y. Tong, J. Vac. Sci. Technol. **12**, 230 (1975).
[138]W. Oed, H. Linder, U. Starke, K. Heinz, K. Muller, and J. B. Pendry, Surf. Sci. **224**, 179 (1989).
[139]H. H. Brongersma and J. B. Theeten, Surf. Sci. **54**, 519 (1976).
[140]J. W. M. Frenken, R. G. Smeenk, and J. F. Van der Veen, Surf. Sci. **135**, 147 (1983).
[141]Th. Fauster, H. Durr, and D. Hartwig, Surf. Sci. **178**, 657 (1986).
[142]J. E. Demuth, J. Colloid Interface Sci. **58**, 184 (1977).
[143]G. Kleinle, J. Wintterlin, G. Ertl, R. J. Behm, F. Jona, and W. Moritz, Surf. Sci. **171**, 225 (1990).
[144]M. Schuster and C. Varelas, Surf. Sci. **134**, 195 (1983).
[145]A. Baro, G. Binnig, H. Rohrer, C. Gerber, E. Stoll, A. Baratoff, and F. Salvan, Phys. Rev. Lett. **52**, 1304 (1984).
[146]R. G. Smeenk, R. M. Tromp, and F. W. Saris, Surf. Sci. **107**, 429 (1981).
[147]H. Niehus and G. Comsa, Surf. Sci. **151**, L171 (1985).
[148]R. Baudoing, Y. Gauthier, and Y. Joly, J. Phys. C **18**, 4061 (1985).
[149]J. F. van der Veen, R. M. Tromp, R. G. Smeenk, and F. W. Saris, Surf. Sci. **82**, 468 (1979).
[150]J. E. Demuth, N. J. DiNardo, and G. S. Cargill, Phys. Rev. Lett. **50**, 1373 (1983).
[151]D. T. Ling, J. N. Miller, P. A. Pianetta, D. L. Weissman, I. Lindau, and W. E. Spicer, J. Vac. Sci. Technol. **15**, 495 (1978).
[152]R. Mayer, C. S. Zhang, and K. G. Lynn, Phys. Rev. B **33**, 8899 (1986).
[153]Y. K. Wu and K. A. R. Mitchell, Can. J. Chem. **76**, 1975 (1989).
[154]Th. Fauster, H. Durr, and D. Hartwig, Surf. Sci. **178**, 657 (1986).
[155]H. Niehaus, Surf. Sci. **130**, 41 (1983).
[156]G. Ertl, Surf. Sci. **6**, 208 (1967).
[157]E. Zanazzi, M. Maglietta, U. Bardi, F. Jona, and P. M. Marcus, J. Vac. Sci. Technol. **1**, 7 (1983).
[158]W. Heiland, F. Iberl, and E. Taglauer, Surf. Sci. **53**, 383 (1975).
[159]J. H. Onuferko, D. P. Woodruff, and B. W. Holland, Surf. Sci. **87**, 357 (1978).
[160]A. L. D. Kilcoyne, D. P. Woodruff, Th. Lindner, J. Somers, and A. M. Bradshaw, J. Vac. Sci. Technol. A **7**, 1926 (1989).
[161]C. Ammer, M. Klaua, and H. Bethge, Phys. Stat. Sol. **71**, 415 (1982).
[162]B. A. Sexton, Surf. Sci. **88**, 319 (1979).
[163]D. P. Woodruff, C. F. McConville, A. L. D. Kilcoyne, Th. Lindner, J. Somers, M. Surman, G. Paolucci, and A. M. Bradshaw, Surf. Sci. **201**, 228 (1988).
[164]D. Arvanitis, K. Baberschke, L. Wenzel, and U. Dobler, Phys. Rev. Lett. **57**, 3175 (1986).
[165]J. E. Demuth, IBM J. Res. Develop. **22**, 265 (1978).
[166]P. Geurts and A. van der Arvoird, Surf. Sci. **103**, 416 (1981).
[167]K. Takayanagi, Y. Tanishiro, M. Takahashi, and S. Takahashi, J. Vac. Sci. Technol. A **3**, 1502 (1985).
[168]T. Ichikawa and S. Ino, Surf. Sci. **136**, 267 (1984).
[169]T. Nurasawa and W. M. Gibson, Phys. Rev. Lett. **47**, 1549 (1981).
[170]H. J. Grossman, L. C. Feldman, and W. M. Gibson, Phys. Rev. Lett. **53**, 294 (1984).
[171]M. Watamori, F. Shoji, T. Hanawa, and K. Ouda, Surf. Sci. **226**, 77 (1990).
[172]G. Le Lay, G. Quentel, J. P. Faurie, and A. Masson, Thin Solid Films **35**, 273, 289 (1976).
[173]M. Saitoh, F. Shoji, K. Oura, and T. Hanawa, Surf. Sci. **112**, 306 (1981); Jpn. J. Appl. Phys. **19**, L421 (1980).
[174]R. J. Wilson and S. Chiang, Phys. Rev. Lett. **58** 269 (1987).
[175]R. J. Wilson and S. Chiang, Phys. Rev. Lett. **59**, 2329 (1987).
[176]E. J. van Loenen, J. E. Demuth, R. M. Tromp, and R. J. Hamers, Phys. Rev. Lett. **58**, 373 (1987).
[177]A. Ichimiya, S. Kohmoto, T. Fujii, and Y. Horio, Appl. Surf. Sci. **41/42**, 82 (1989).
[178]M. Copel and R. M. Tromp, Phys. Rev. B **39**, 12688 (1989).
[179]E. Vlieg, A. W. van der Gon, J. F. van der Veen, J. E. McDonald, and C. Norris, Surf. Sci. **209**, 100 (1989).
[180]E. J. van Loenen, J. W. M. Frenken, J. F. van der Veen, and S. Valeri, Phys. Rev. Lett. **54**, 287 (1985).
[181]R. J. Meyer, C. B. Duke, A. Paton, J. C. Tsang, J. L. Yeh, A. Kahn, and P. Mark, Phys. Rev. **22**, 6171 (1980).